Vision-Augmented Molecular Dynamics Simulation of Nanoindentation

Rajab Al-Sayegh

A thesis submitted for the degree of Doctor of Philosophy in Mechanical Engineering

Brunel University London

Department of Mechanical, Aerospace and Civil Engineering, College of Engineering, Design and Physical Sciences

March 2016

Abstract

This thesis has contributed to the literature by providing a pathway to simplify the process of carrying out molecular dynamics simulation. As a part of the investigation, a user-friendly vision-augmented technique was developed to set up and carry out atomistic simulations using hand-gestures. The system is novel in its concept as it enables the user to directly manipulate the atomic structures on the screen, in 3D space using hand gestures, allowing the exploration and visualisation of molecular interactions at different relative conformations. The hand gestures are used to pick and place atoms on the screen allowing thereby the ease of preparing and carrying out molecular dynamics simulations in a more intuitive way. The end result is that users with limited expertise in developing molecular structures can now do so easily and intuitively by the use of body gestures to interact with the simulator to study the system in question.

The proposed system was tested by performing parallel molecular dynamics simulations to study (i) crystal anisotropy of a diamond cubic substrate (crystalline silicon) using nanoindentation with a long-range (Screened bond order) Tersoff potential and (ii) crystal anisotropy of a body centre cubic metal (tantalum) using nanoindentation with an Embedded Atomic Method (EAM) type potential.

The MD data was post-processed to reveal size effects observed in anisotropy of both these materials, namely, silicon and tantalum. The value of hardness and elastic modulus obtained from the MD data was found in accordance with what has been discovered previously by experiments, thereby validating the simulations. Based on this, it is anticipated that the proposed system will open up new horizons to the current methods on how an MD simulation is designed and executed.

Acknowledgements

If the completion of a PhD study is all about persistence than it was a major challenge to complete this study without the inspirational guidance and support of many individuals. Although the list of people, whom I wish to express my deepest gratitude, far exceeds the words, there are certain individuals who deserve special mention for their care, motivation, guidance, support, and encouragement.

At the outset, I would like to express my deepest gratitude to **Dr. Charalampos Makatsoris** who was always on my side with moral, intellectual, and material support particularly in the overall preparation and presentation of the thesis content**.**

In addition, I would like to thank my loving father and mother who ensured that I did not lack anything during this critical part of my academic life and gave me the most valuable words of encouragement during the entire course of the study.

Furthermore, I would like to thank my friends **Muhannad Alalwan, Harron Ahmad, Rashid Qazi, Abid Rafique, Mohammed Saafi, Abdulrahman Al-Harethi, Fahad Alawi, Bilal Akbar, Mohannad Jreissat** and last but not least **Omar Shariff Khan** for their help and support during my PhD life.

I cannot also forget to mention my loving brother and sisters, **Ghassan, Jacqueline** and **Maha** whose inevitable disturbances and encouraging smiles served to relax my mind.

To you all, whom I have not mentioned, I cannot thank you well except to say that, **May Allah bless you in all your endeavours**.

The author acknowledges the funding support of **King Abdullah bin Abdul-Aziz Al-Saud** (may Allah be merciful to him), Ministry of Higher Education and Northern Borders University, Kingdom of Saudi Arabia for funding this PhD research.

Declaration statement

I hereby declare that this piece of research work has not been submitted within a degree program in support of an application for another qualification or degree programme at this or any other institution. I also declare that, this work has been written by me and I am responsible for the work submitted in this thesis.

Signature: ----------

Date: ----------

Table of Contents

Abstract i
Acknowledgements ii
Declaration statement iii
List of Tables vi
List of Figures vii
Abbreviations and Definitions viii
Nomenclature ix
List of Publications by the Author x
Chapter 1 - Introduction 1
1.1 Background and significance 1
1.2 Aim and objectives of the research 3
1.3 Structure of the thesis 4
Chapter 2 - Literature review of computer vision and virtual environment 6
2.1 Introduction 6
2.2 The advantages of using computer vision and virtual environments 7
2.3 Haptic Device Application and Visualisation in Molecular Dynamics 10
2.4 Examples of using Haptic Device 14
2.5 Virtual Reality and Haptic Applications 16
2.6 Virtual Reality for Molecular Dynamics 18
2.7 Summary 22
Chapter 3 – Review and theory of MD simulation of contact loading 23
3.1 Concept, introduction and background 23
3.2 Contribution of MD to the field of contact loading problems 24
3.3 Potential energy function 25
3.4 Preparations for the MD simulation 32
3.5 Post processing of results 35
3.5.1 High pressure phase transition in silicon like materials 35
3.5.2 Calculation of stresses 37
3.5.3 Calculation of the temperature in the indentation zone 38
3.6 Summary 39
Chapter 4 – Vision-augmented molecular dynamics simulation 40
4.1 Introduction 40
4.2 Generic scheme of performing vision-augmented MD 40
4.3 Functional Descriptions 43
4.4 The Gesture App 44
4.4.1 Gestures Detection Using NITE Algorithms 47
4.4.2 Mouse Control using Right Hand Movement 47
4.4.3 Customized Algorithm for Left Hand Gestures Detection 48
4.4.4 Mouse Control using Left Hand Movement 49
4.4.5 Connection with the JMOL Visualizer and Gesture App 49
4.4.6 Gestures to JMOL Command Conversion 50
4.5 The Jmol Visualizer 51
4.6 Open Visualisation tool (OVITO) 51
4.7 Scripting Framework 52
4.8 Summary 53
Chapter 5 - VAMDS results for the nanoindentation of silicon 54
5.1 Introduction 54
5.2 VAMDS results on single crystal silicon 54
5.2.1 Methodology of VAMDS of nanoindentation of silicon 54

5.2.2 Calibration of the VAMDS system for nanoindentation of silicon 59
5.2.3 VAMDS results on nanoindentation of silicon 60
5.3 Summary 68
Chapter 6 - VAMDS results for the nanoindentation of tantalum 70
6.1 Introduction 70
6.2 Brief review of literature on contact loading of tantalum 70
6.3 VAMDS methodology for nanoindentation of tantalum 72
6.3.1 Calibration of the VAMDS system for nanoindentation of tantalum 76
6.4 VAMDS results for nanoindentation of tantalum 78
6.5 Summary 82
Chapter 7 - Conclusions and future work 84
7.1 Conclusions of the research 84
7.2 Research contributions 86
7.3 Recommendations for future work 87
7.3.1 Development of a force field or a potential function 89
7.3.2 Manual creation of defects and study of wear 90
7.3.3 Development of enhanced MD software 90
7.3.4 Effects of coolant and coatings 90
7.3.5 Optimization of indentation probe 90
7.3.6 Sensitivity and least count of the haptic device 91
References 92

List of Tables

Table 3-1: Morse potential for metallic systems [50] 26
Table 3-2: Tersoff potential parameters for silicon [51, 52] 28
Table 3-3 : Tersoff potential parameters for silicon and carbon alloys 30
Table 3-4: Potential function parameters of silicon and carbon [58] 31
Table 4-1: Gestures to JMOL Command Mapping 51
Table 5-1: Details used for the development of MD simulation model 57
Table 5-2: Computational results obtained from the nanoindentation simulation 65
Table 6-1: Details used for development of the MD simulation model 75
Table 6-2: Summary of results obtained from the MD simulation (P-h plots) 82

List of Figures

Figure 3-1: Principle of molecular dynamics simulation [43] 23
Figure 3-2: Brittle-ductile transition in silicon as a result of change of temperature [48] 25
Figure 3-3: The increasing cost of processing power in seconds/atom/time step for state-of-the-art potential functions [49] 26
Figure 3-4: Schematic of MD simulation model 33
Figure 3-5: Periodic boundary condition [65] 34
Figure 3-6: Illustration of MD (a) The initial positions of the molecules are specified (b) Force on each atom due to the other atoms in its neighbourhood is calculated. (c) Potential energy function predict the newer positions and velocities of the atoms at a specified time [66] 35
Figure 3-7: Schematic diagram of radial distribution function [71] 37
Figure 4-1: Vision-Augmented Molecular Dynamics Simulation 42
Figure 4-2: The integration between Computer vision and Molecular Dynamics Simulation 42
Figure 4-3: Sequence diagram for VAMDS 43
Figure 4-4**:** Microsoft Kinect 44
Figure 4-5: OpenNI and NITE Framework for Gesture Recognition [2] 46
Figure 4-6: Wave Gesture [1] 47
Figure 4-7: Gestures Recognition (Only Steady, SwipeLeft, SwipeRight and Push Gestures are shown for the Left Hand) 49
Figure 4-8: Communication between the GestureApp and other modules. 50
Figure 4-9: Scripting Framework 53
Figure 5-1: Schematic of the MD simulation model of silicon 56
Figure 5-2: Comparison of physical movement with the movement in the MD simulation model (a) at the beginning of the simulation, (b) when the indenter establishes contact with the substrate and (c) final indentation depth was achieved. 59
Figure 5-3: Relationship between physical movement of hand gesture and indenter in the MD model 60
Figure 5-4: Cross-sectional view of the silicon substrate in the XY plane highlighting the change in coordination number at peak indentation depth of 2 nm on three orientations 62
Figure 5-5: P-h plots of the nanoindentation for all three crystal orientations of silicon 63
Figure 5-6: Variation in the (a) elastic modulus and (b) nanoindentation hardness of silicon with respect to the indentation depth 67
Figure 6-1: Schematic diagram of MD simulation model of the nanoindentation of tantalum. 73
Figure 6-2: Comparison of physical movement with the movement in the MD simulation model (a) at the beginning of the simulation, (b) when the indenter establishes contact with the substrate and (c) final indentation depth was achieved. 76
Figure 6-3: Relationship between physical movement of hand gesture and indenter in the MD model 77
Figure 6-4: P-h plots obtained from the MD simulation for the three cases using rigid tantalum indenter 78
Figure 6-5: Manually performed comparison between VAMDS with a purely repulsive indenter on the (010) orientation of tantalum by keeping all the indentation parameters same but using two different kind of indenters (i) using a rigid tantalum indenter by VAMDS and (ii) a purely repulsive indenter simulated without VAMDS 79
Figure 6-6: Variation in the (a) elastic modulus and (b) nanoindentation hardness of tantalum with respect to the indentation depth 80

Abbreviations and Definitions

FRODA	Framework Rigidity Optimised Dynamic Algorithm
GestureApp	Application which convert gestures to commands
HPC	High performance computing
IMD	Interactive molecular dynamics
JMOL	Java viewer for molecules in 3D
MD	Molecular dynamics
NITE	Interaction for End-user
NVE	Microcanonical ensemble
OVITO	Open Visualization tool
PBC	Periodic boundary condition
TEM	Transmission electron microscope
VAMDS	Vision-augmented Molecular Dynamics Simulation
VMD	Visual molecular dynamics

Nomenclature

a	Contact radius of the spherical indenter
A	Projected area
B	Bulk modulus
C_{ij}	Elastic constants of the material
E or E_s	Elastic modulus of the material
F or P	Normal force or load on the indenter
G	Shear modulus
h	Instantaneous displacement of the indenter
h_f	Residual depth of indentation
h_{max}	Maximum depth of indentation
H	Hardness of the material
K	Force constant
P-h	Load-displacement curve
p_m	Contact pressure
R	Radius of the indenter
r_0	Cutoff radius between indenter and the substrate material
S	Slope of the unloading curve
$\sigma_{hydrostatic}$	Hydrostatic stress
σ_1, σ_2 and σ_3	Principal stresses
ε	Strain
τ	Shear stress
σ_y	Yield stress for plastic flow

List of Publications by the Author

International Journal:

- Rajab Al-Sayegh and Charalampos Makatsoris, "Vision-Augmented Molecular Dynamics Simulation of Nanoindentation," Journal of Nanomaterials, vol. 2015, Article ID 857574, 11 pages, 2015. doi:10.1155/2015/857574

International Conference Proceedings:

- R. Alsayegh, L. Paramonov and C. Makatsoris. A novel virtual environment for molecular system design. Computational Intelligence and Virtual Environments for Measurement Systems and Applications (CIVEMSA), 2013 IEEE International Conference on: IEEE, 2013. p.37-42.

- Research Conference 2013 (ResCon) held at Brunel University

- Research Conference 2012 (ResCon) held at Brunel University.

Poster Presentations:

- Presented an invited poster at the 6th Saudi Scientific International Conference that was held at Brunel University, 1th – 14th October 2012 Sponsored by King Fahd University of Petroleum and Minerals.

Chapter 1- Introduction

1.1 Background and significance

Computational simulation approaches such as Molecular Dynamics (MD), Monte Carlo or coarse grained MD, are widely employed by chemists and materials scientists to predict and understand the behaviour of materials despite the fact that they are computationally expensive. Such computationally expensive simulations at the moment are somewhat a black-box since the user never gets to know as to what happens during the simulation. Therefore, there is a necessity to develop a virtual environment tool that can offer exploration of complex energy landscapes by allowing the user to directly interact with the simulated molecular system.

One of the pathways to achieve such a virtual environment would be via the use of haptic devices since they have already commercially been used for gaming technology, multi-media, robotics, etc. Microsoft has introduced Kinect in November 2010 [1] in order to broaden its Xbox technology from key board input to gesture based input. Kinect includes the features of gestures recognition, facial recognition and voice recognition. The Kinect camera depth sensing technology is developed by Prime Sense which has also released an open source motion tracking middleware Natural Interaction for End-user (NITE). NITE application programming interface (API) is used to control various functionalities of Kinect. The NITE algorithm provides scene segmentation, hand point detection and tracking, and full body tracking features. The NITE framework provides the developer an application programming interface (API) which includes methods for controlling the user interface.

There are several other similar projects focussed on introduction of gaming devices as a concrete tool to support teaching and learning activities. They can be considered the forerunners in the type of problem investigated in this thesis. They constitute the

starting point of this thesis and an important inspiration on the approach we needed to elaborate a concrete solution to this specific problem. In November 2010 Microsoft has released what they define “the birth of the next generation of home entertainment”. Microsoft did not know at the time of the launch the fact that Kinect is not just a “common" game device, it is rather so much more. It is a new technology and a new paradigm of interaction, it renders legacy external peripherals currently used today, such as remote controls, keypads or a mouse obsolete. It originated a lot of interest by the entire Information Technology (IT) world. Indeed on the Web were appeared rapidly a lot of “hacks" and university projects that highlight the potentiality of a technology of this kind. Many of these projects were supported by the frameworks provided by the creator and precursor of this new paradigm of interaction called “PrimeSense" [2] which was the first to publish stable frameworks to interact and develop Kinect-based application. Microsoft itself has noted this phenomenon and released a non-commercial Kinect Software Development Kit (SDK) for Windows in June 16, 2011. Kinect can be defined a Natural Interaction (NI) device, which operates in the context of Natural User Interface (NUI), a new emerging metaphysical paradigm in Human Computer Interaction (HCI). NI refers to a concept whereby the interaction with devices is based on human senses. The main goal of the NI paradigm is to transform the legacy interfaces and devices used during the last years of technology evolution in a more intuitive and naturally interaction without the need to wear particular devices or learn complicated instructions to use them. The Kinect can perfectly play this role in the process of transformation and it is this idea that resulted into a thought to use Kinect device for performing molecular dynamics simulation (MDS) in this work.

1.2 Aim and objectives of the research

As discussed in section 1.1, the aim of this work is to perform the "Interactive MD" which would allow real time visualization and manipulation of MD simulations through the use of haptic device similar to the IMD protocol which was first implemented in VMD and NAMD. Specifically it allows the MD program to monitor the progress of the simulation and interactively apply forces to selected atoms. Aside from this, the exploration to use the haptic devices to perform molecular dynamics simulation will make the non-expert MD users to perform the computer simulations in a more efficient and accessible way by eliminating the need of writing complicated scripts for geometry creation. Hence, this research will evoke interest of individuals in performing MD simulations as well as perpetuate its advancement in teaching. Hence, the ultimate aim of this research is to reach Multi Scale Approach by integrating computer vision (e.g. Gesture recognition & Artificial intelligence), Molecular Dynamics (e.g. Molecular modelling & Material modelling) and intuitive understating of atomic scale. By doing these, we will be able to interact with molecules via our gestures, for example, by using our hand gestures to deal with molecules. To accomplish this task, a Vision-Augmented Molecular Dynamics Simulation (VAMDS) technique was developed to deliver a number of specific outputs. Aside from performing MD simulation, a complete hardware design setup was developed for thorough testing. In order to achieve this aim, following objectives were set:

- Make the design of materials and processes via atomistic simulation more accessible to inexperienced users.
- Introduce defects in the molecular structures or design and develop novel materials with ease merely by the use of hand gestures instead of scripting the coordinate geometry of the molecules.

- Using an intuitive approach to perform simulations aimed at designing novel materials
- Introduce a new methodology that will allow the design and execution of MD simulations in a more interactive manner with the expert user in the loop
- Provide a new method that allows for the in depth understanding of atomic scale processes with novel visualisation techniques.

1.3 Structure of the thesis

This thesis is divided into the following seven chapters:

Chapter 1 explains the relevance of the research in the current context of thesis and describes the major objectives of this work.

Chapter 2 reviews the various kinds of hardware and design systems developed so far for using haptic devices. It highlights the advantages of using computer vision and virtual environment in real life by taking into consideration the use of haptic device in the context of molecular dynamics simulation. The chapter shows some of the unique examples of using Haptic Device by researchers particular in the context of virtual Reality in Haptic Applications and in Molecular Dynamics.

Chapter 3 describe the basic concept and framework of the MD simulation approach. This follows with a discussion about the importance of the potential energy function, something which has not received any attention in previous studies. This chapter also provides a detailed description of the tools required for pre-processing and post-processing of the MD simulation results.

Chapter 4 demonstrate the design and development of the haptic device by first giving the details of the hardware used in this work and thereafter providing the details of the software. The particular thing to notice from this chapter is the integration of hardware

and software making use of only open source codes for easy accessibility and flexibility of modification by any user in the future.

Chapter 5 describes how the proposed concept of VAMDS was successfully adapted as a useful tool to investigate the crystal anisotropy of diamond cubic lattice structures material called silicon. Along with a comprehensive discussion on the high pressure phase transformations of the silicon, this chapter provides detailed quantitative insights on the anisotropic variation observed in silicon. The chapter also covers the variation observed in the P-h plot, elastic modulus and hardness of silicon.

Chapter 6 describes how the proposed concept of VAMDS was successfully adapted to undertake another case study to study the anisotropy in a body centred cubic (BCC) metal tantalum (Ta). Oliver and Pharr method was applied to the load-displacement (P-h) plots obtained from the simulation as a mean to quantify the observed anisotropy. Much like previous chapter a good correlation was obtained between the simulation results and the previously published and known experimental values of mechanical properties extracted from the simulation for Ta.

Chapter 7 presents the assessment and conclusion of the whole research. Based on the simulations developed in the thesis, some measures for improvement as well as some recommendations for work that could usefully be done in the future are made.

Chapter 2 - Literature review of computer vision and virtual environment

2.1 Introduction

Researchers have explored the use of haptic devices in various applications over the last 20 years [3]. The use of haptic devices in molecular dynamics is a novel concept and is the main focus of this research. Molecular dynamics simulations with haptic devices can provide the comfort to the users to interact with the molecules in a more intuitive way to understand the material behaviour in a fully virtual environment. Aside from this, the exploration to use the haptic devices to perform molecular dynamics simulation will make non-expert users to perform the computer simulations in a more efficient and accessible way by eliminating the need of writing complicated scripts for geometry creation. One of the main advantages of the use of haptic devices in the simulation framework is that (i) it offers potentials to provide more in-depth understanding of body-to-body interactions and (ii) user directs execution of MD simulations by eliminating waste of time by the computer setting to achieve specific states such as equilibration.

Vision tools provide a more scientific rational to perform the simulation on a sound design footing with the aid of advanced techniques involving the use of haptic devices. The applications of haptic devices include games technology, multi-media, robotics, molecular dynamics, etc. Human gestures recognition is an important task where haptic devices are used. Kinect includes the features of gestures recognition, facial recognition and voice recognition. The Kinect camera depth sensing technology is developed by Prime Sense which has also released an open source motion tracking middleware NITE. Natural Interaction for End-user (NITE) application programming interface (API) is used to control the Kinect various functionalities. The NITE algorithm provides the

scene segmentation, hand point detection and tracking, and full body tracking. The NITE framework provides the developer to control user interface.

Such a research is remarkably challenging and innovative because it will open up new horizons for development and knowledge by building a clear base from which development of the computer vision would enable the design and creation of new materials.

2.2 The advantages of using computer vision and virtual environments

Researchers at MIT Media Lab [4] have produced a wearable gesture interface which used a small camera and a projector. The purpose of the device was to interact with the real world objects. The system recognises freehand gestures like hand waving, multi-touch systems like shapes with both hands and iconic gestures like in air drawing. The system can be worn on the cap having a unique feature of mobility. The camera sees the environment as the user and takes the user gestures commands using computer vision techniques and the project visualise the required output on any surface and allows the user to interact. Examples include interactive map, a watch on hand, zoom in/out newspaper, etc. The group has done a lot of novel work in the haptic devices.

Fermeglia et al. [5] analysed molecular structures on nano scale of 0.1-10 nm using atomistic-based simulations such as molecular dynamics, molecular mechanics and Monte Carlo-based methods. Since these methods are now widely used in material design and molecular dynamics simulations, the fast and precise prediction of new computational material properties is needed before they can be further developed and produced effectively. This is especially important where material properties are dependent on their nanostructure, such as in the field of polymer nano-composites. Svaneborg et al. [6] used LAMMPS for calculating directional and dynamic bonding by separating bonded and non-bonded interactions. Aragones et al. [7, 8] developed extra libraries in LAMMPS for simulating the intermolecular free energy potential and

compared the results with the experimental data. Mistry et al. [9, 10] have worked on combining handwritten notes with digital contents like emails, calendar, etc. They have developed a ‘Quickies’ system which reads the sticky notes input and gives digital output on your device. If you put a meeting with a person at 3 pm on a sticky note, it automatically updates your calendar and reminds you before that. The system is mainly composed of sticky notes, digitizer pad and software on output device. The users write on sticky notes by placing it on the digital pen and pad device. The digitiser stored it in computer by using hand writing recognition algorithms. The software also categorised the notes based on their types like meeting, To-do list, message, reminder, etc. The output can be seen on any of the device like mobile phone, photo frame, computer, etc. Besides of natural language processing, Quickies is intelligent enough to take graphical input like a chart/ graph and store it an image. This work is very useful as it attempts to bridge the gap between physical and digital world.

The researchers have also developed [11] a hand free input interface for controlling and commanding a robot. The glaze and blink input directs the robot to move an object from one location to other. The ‘Blinkbot’ replaces the traditional interactive devices like mouse, keyboard and speech based input systems which are not very good at directional input in space. With the Blinkbot wearable controller, user gives input by gaze need a gaze to select an object and actions are triggered by a blink. The action is to move the object to a desired location by the robot. This is a novel technique which provides highly interactive sense of touch and can be used to help disabled people.

They have presented techniques to collaborate the computer aided design (CAD) tools and handmade pencil and paper based designs. Two and three dimensional CAD tools are widely used in engineering and architecture design and required skills to use them effectively. Some of the designer still like the traditional paper based design tools. In addition, hand drawn object placed on frosted glass surface is tracked by ultrasonic

digital pen hardware. Pen tip transmits the ultrasonic waves which are received by two stationary sensors and time of receiving wave helps to find the location of the tip. There are set of infrared sensors on the pen tip which are detected by two cameras with IR filter and help to calculate the X-Y-Z coordinates of the pen by triangulation method. The software performs the data processing and computer displays the 3D view of the object. This novel technique will open a new horizon of CAD design.

Mistry et al. [10] also developed a LCD/CRT display which provides different contents for different viewers wearing 3D shutter glasses simultaneously. The system actually switches between transparent and opaque as when one viewer is transparent, other is opaque at frame rate of 120 Hz. At higher frame rate more viewers can be added. This is a good technique but it requires wearing a special glasses. Mistry et al. [12] developed a 'Mouseless' system that replaces the computer mouse. The system is composed of infrared camera and infrared laser beam sensor. The system detects the movement of the hand, moves the computer cursor accordingly and also performs right, left click and scroll operations. Taylor et al. [13] proposed a haptic interface in which parameters of the computer simulations are controlled by physical means like robots. The demonstration of tangible simulation is performed by three body gravitational simulation.

Ricci et al. [14] used haptic devices in the arena of computer aided drug design. Haptic driven simulators provided the user opportunity to drive and control simulation, increased interactivity and combined the human knowledge and computational power. The researchers were optimistic of using new advanced haptic devices like Microsoft Kinect and other sensors in future research. Dreher et al. [15] have connected 3D virtual reality environment with molecular dynamics simulator, Gromacs, where forces applied to haptic devices were used to select the atoms for steering large scale MD simulations.

The simulation framework composed of selector, powerful multi core processors and visualizer.

2.3 Haptic Device Application and Visualisation in Molecular Dynamics

In the past various researchers have attempted to work on the Haptic device development and these have been summarised in this section. Aside from this narrative summary the chapter concludes by highlighting the shortcomings and advantages of the device development in this work. Haag et al. [16] have studied the chemical reactivity by using the intuitive virtual environment manipulation techniques. Due to high cost of quantum chemical calculations in regard to their computational efforts, they have re-introduced the tools which provide immediate feedback and good manipulation capability. In addition to this virtual environment was used to explore the reaction mechanism, study of reaction networks and to analyse the scaling of the forces. In short VE tools will increase the creativity in the chemical reaction.

Chen et al. [17] have developed an interactive virtual environment for nanoparticles simulation and 3D visualisation. Virtual reality provides real time manipulation MD structures like interacting with real objects. The proposed system software is composed of interactive virtual environment module for manipulating a nanoparticle, device interface module for controlling a virtual single-tip nano-manipulator and molecular dynamics calculation module to determine the trajectory of a manipulated nanoparticle. The models of the nanoparticle are loaded via Pro-Engineer software and EON studio is used for VR presentation. The visualisations are rendered on the computer screens. The authors used the mouse and touch pad input in device interface module which are not easy to manipulate.

Glowacki et al. [18] have described a framework composed of software algorithms and hardware that are used for interactive molecular dynamics using an array of consumer

depth sensors. Ten depth sensors were used to create an immersive 360 degree space utilising GPU acceleration which allows multiple users to simultaneously chaperone the dynamics. The platform was flexible enough to carry out molecular dynamic simulations which were considerably enhanced by the wrappers that facilitated fast communication with a portable selection of GPU-accelerated molecular force evaluation routines. In this paper, the proposed 360 degree atmospheric molecular dynamics simulation model was used in education context.

Waldon et al. [19] developed a tool SketchBio in order to create three dimensional models and animations. This has helped them to avoid in house custom developments for visualising molecular structures. It has unique features of crystal for example, pose mode physics and spring based layout which provides acceleration in the formation of molecular models. The tool provides the gestures and speech based user interface in order to interact with molecules using Kinect device. To speed up the rendering of interactive object on screen, the actual objects were replaced by simpler geometry imposter which has drastically increase drawing process of complex structure. The tool also uses the bimanual controller which provides 6 degree of freedom tracker, various buttons and an analogue input. The tool has the capability of dropping shadows to improve depth perception, rapid collision detection, real-time preview and spline interpolation.

Heinrich et al. [20] evaluated the application of 1D, 2D and 3D visualisation techniques used for exploring molecular structures. The molecules can be modelled in three dimensions point cloud using spatial position of their atoms. They have demonstrated the use of interactive devices like 3D mice, Leap motion controller and phantom haptic devices to control the motion of the macromolecular structures. These interactive devices helped them better understand the structure although there is big demand for further research in this area for understanding the complex data.

Ferey et al. [21] used the interactive techniques in order to fully observe the dynamics of the macromolecules at atomic details level which is difficult to observe using traditional molecular dynamics simulation techniques. They developed libraries in order to interact with simulation engines like GROMACS or NAMD and VTK based user interface for interaction. They have used haptic paradigm to interact with various molecular simulation engine with varying molecular dynamic models and accessing different time scales which has helped them improve simulation methods. Apart from their benefits, interactive molecular dynamics has some constraints like interactivity to several thousand atoms, visualisation for the moving scene but these limitations can be reduced by optimisations and further research.

Bolopion et al. [22-24] developed novel molecular simulator using haptic device which performed variety of manipulations. Both position and force control is implemented in the tool which simulate systems with hundreds or thousands degrees of freedom. To understand the nano-scale phenomenon, a haptic device is connected to simulator. For getting haptic feedback, they have studied various methods like Bubble technique, Active Haptic Workspace. The tool was used to manipulate whole molecules to modify the global structure of the molecular system, deformation of the molecular structures in order to measure their inherent properties and the determination of equilibrium positions. The tool has the capability of adding or removing more atoms to design new molecular structures where haptic feedback assisted the user to break the energy barrier.

Sun et al. [25] designed a molecular visualisation interactive environment (MOLVIE) to display three dimensional structures of proteins for analysis and research. MOLVIE was developed in JAVA and can be accessed from the web page where it runs as an applet. MOLVIE editor can be used to construct new molecules and help user to explore inner part of molecular structure. It can load two molecules simultaneously and display them into a window. MOLVIE can re-compute co-ordinates of the partial atoms, bonds and

re-contract the molecular structure after user modifies the molecular structure interactively. The object oriented programming style of MOLVIE made it suitable for embedding into other applications. Due to limitations of the JAVA platform, MOLVIE does not support huge molecules and does not output images.

Hirst et al. [26] reviewed the virtual immersive molecular simulation, advanced visualisation and analytics techniques, application and model building and new developments in high performance computing. Initially interactive simulations systems had used sense of touch but later on audio and visual feedback sensory channel were used to create immersive effect. An interactive molecular simulation framework requires a screen based mechanism to visualise molecular structure, interactive devices like mouse, camera, haptic sensors, etc, physics based simulation engine and a network protocol often with low latency coupling. Interactive simulations are supported by currently available software like LAMMPS, NAMD, HOOMD, ProtoMOL and OPEP/Hi RE-RNA. Parallel computing and use of GPU provides the animation a high frame rate over 24Hz. The large amount of molecular simulation data creates bottleneck for interactive devices and visualisation. But the introduction of GPU in various molecular dynamics software like GROMAC, AMBER has accelerated the execution time and increased the scalability. In short, new hardware structures, software platforms, interactive devices has improved the molecular dynamics simulation framework and opened potential for new research. As it can be seen while various efforts are made towards the device development, they are either computationally expensive, have either outdated, are not economic or have either failed to absorb the growing and challenging requirements of the users. Consequently, some later developments have led to the use of Microsoft Kinect device which has been summarised below.

2.4 Examples of using Haptic Device

Microsoft Kinect has been used in engineering applications by researchers in addition to its typical application in games consoles. Sharma et al. [27] have used the Kinect sensor to estimate the correct depth of the video scene. Microsoft Kinect sensor has relatively high frame rate which recognises the user gestures and human poses. Authors have extracted features from the video signal and developed algorithms using Neural Networks for pattern matching. They have proposed the solution for the robotics applications but the Kinect camera has the potential of using in other application as we have used in molecular dynamics interaction. The SIFT method was used to calculate the descriptor vector and then self-organising map (SOP) was used to estimate winning pixels. The proposed method has provided efficient feature matching between successive frames and can be used in various computer vision applications.

Wang et al. [28] developed a different hand gestures recognition method using Kinect sensor. They used OpenNI to locate the palm position and Hidden Markov Model (HMM) technique to track gestures. After training the HMM, their system recognises the gesture sequence and compared it with previous results. Since palm is defined as a hand node in Prime Sense's OpenNI platform, hence it was used for Kinect application development. The method has significantly improved the gesture track recognition rate. The process is composed of gesture modelling, gesture analysis, and gesture recognition and computer results. HMM was trained by seven different gestures left, right, up, down, "S", "O", "E" with sample size of thirty for each type. Since the position and speed of the gesture may vary at different instances, but the tangent angle remains almost the same for each type of the gesture hence it is extracted as a feature for training HMM. The real time recognition rate among the most of the seven gestures was over 90% which is better than the traditional hand gesture techniques.

Han et al. [29] presented a comprehensive review on the computer vision algorithms and application using low cost, high resolution Microsoft Kinect sensor. They have compared the most of the topics related to computer vision which include pre-processing, object tracking and recognition, human activity and gesture analysis and indoor 3D mapping. Because of the ability of giving synchronised RGB colour and depth image data, and contact less interaction between user and environment, they have used the Kinect sensor. The depth measurement of the scene in the Kinect is performed by the infrared (IR) projector and infrared camera where the former casts IR speckle dot pattern into the 3D scene while the later captures the reflected IR speckles. The performance of the Kinect sensor was observed better than the Stereo and TOF camera. The Kinect sensor data need to be pre-processed before sending it to computer vision algorithms. The pre-processing step is mainly composed of spatially aligning the RGB camera output and depth camera output. The object racking and recognition using Kinect depth sensor has solved the traditional background subtraction problem. Hand detection and tracking by fusing the RGB colour image and depth data provides accurate results. Kinect provides the pair wise point alignment of the depth images combines with sparse features extracted from RGB images, then optimised to get 3D mapping of the scene.

Raheja et al. [30] used MS Kinect to track the finger tips and palm centre. The depth vector of Kinect was used to detect hand whereas centres of palm were detected by the transformation on inverse image. Finger tips detection algorithm first detects the palms of the hand and then used the circular filter to remove the palm which results in segmented fingers. The segmented fingers multiplied with original depth image to get the depth map which were analysed to get the finger tips position. The finger tips detection accuracy was nearly 100% for open fingers but for bended finger it was reduced as system got confused. Similarly the palm centre detection accuracy was up to

90%. This method does not use any gloves or marker on hand and can be applied on controlling the robot movements in the hazard environment.

2.5 Virtual Reality and Haptic Applications

Simulation software and virtual reality devices can be combined due to the ability of high performance computing and high resolution graphics. Novák-Marcinčin [31] demonstrated the use of these combined systems in manufacturing environment and simulation of molecules in chemistry. In manufacturing it can be used in training, collaborative product design, business process design, facility management and many more. To achieve the immersive virtual reality environment hardware and software should be quick enough to take the input and process the output for display without losing the feel of reality. Examples of virtual reality software are 3D Studio, World Tool Kit, Open Inventor, Performer, CAVE, and Division Library. The ISO standard for Virtual Reality Modelling Language (VRML) has been implemented by some software now.

Hamza-Lup et al. [32] presented the web based 3D haptic paradigm for e-learning and simulation which can be used for knowledge sharing. They have proposed the use of X3D and/or web native HTML and JavaScript and haptic devices based tools for providing user interaction. X3D based graphical user interface (GUI) provides the user interaction in three dimensional display, volumetric controls, ability to drag, rotate, or actuate using designated sensors. In HTML and JavaScript based GUI, it is difficult to handles the dynamics of virtual objects in 3D. But if it is combined with X3D, it will solve part of the problem but sometimes synchronisation between them is a problem. The haptic devices like Omni PHANTOM can also be used for interaction the virtual object on the web because of having an open source Application Programming Interface

(API). The example applications of 3D web based simulator are 3D Radiation Therapy Training (3DRTT) and HaptEK16 for learning Pascal principle which mainly uses X3D. Cave automatic virtual environment (CAVE) based immersive virtual reality environment were used by some researchers for molecular dynamics visualisations. Salvadori et al. [33, 34] evaluated the graphical interfaces and virtual reality applications in the molecular science. They divided the visualisation paradigm into two models; all atoms models and backbone model. The all atoms models are representing the molecular structure by ball/ sphere and stick/ cylinder where a ball is atom and a stick is the bond between adjacent atoms. The different radii of spheres and colours were used in order to distinguish different types of bonds and atoms. In backbone model instead of drawing all the atoms, only subset of them are shown which helps them distinguish different motifs in a large molecular structure. For interactive visualisations, they have used state of the art integrated system Caffeine which is developed by using the open source toolkits like OpenSceneGraph, OpenBabel and Qt. These libraries provide the 3D Desktop virtual reality equipped with stereoscopic display and immersive VR environment like CAVE. The system used the GPU based direct volume rendering algorithm in order to manipulate the three dimensional texture data. They have used the absorption plus emission optical model algorithm which assumes that certain density molecules can both emit and absorb incoming light. The mapping between data values and optical properties was encoded in an additional texture and accessed by dependant texture lookup. This algorithms works well but still need some improvements in rendering and ability to handle large datasets.

Xu et al. [35] developed an immersed visualisation environment in CAVE for nano-indentation simulation of Cu. 396,592 atoms were modelled by them using the molecular dynamic simulation. The objective of the system was to visualise the extra ordinary atoms. They have used the integrated approach to visualise the molecular

simulation. They want to overcome the common problems of data pre-processing and feature extraction, scalable parallel processing, and optimisation of basic graphics functionality and visualisation management. They have divided the atoms of the molecules based on their importance and important atoms are visualised by high resolution polygons. CAVE based system has the ability of rendering atoms with low resolution during fast navigation. The users have provided the good feedback of the system which has paved the way of exploring the collaborative large scale MD simulation in tele-immersive networked environment.

2.6 Virtual Reality for Molecular Dynamics

Virtual reality systems have been applied in various molecular dynamics applications. Vormoor [36] discussed how the interactive molecular dynamics has changed the study of molecular structure in the last few decades from traditional command line simulation programs. He studied the colloidal particle dynamics using 3D visualisation techniques. The client-server architecture was proposed along with a protocol for messaging between simulation and visualisation host system which help them change parameters during simulation running. Java3d was used for visualisation which uses the virtual objects having some specific geometry and appearance. Java3d is good for quick and easy visualisations but not good for high end visualisation with optimal performance. JIMD can be used for visualisations with optimal performance for particles up to 400 to 500 and display them as spheres.

Son et al. [37] developed an interactive molecular dynamics simulator which allows user interactions via haptic devices. They used PHANTOM haptic device for push and pull operations which was the integrated part of the system. The system was designed to articulate the behaviour of the structure in real time using user interaction. They were working on resolving the problem of distinguishing the secondary haptic contact in the occurrence of primary haptic contact.

Bolopion et al. [22] developed an adaptive simulation software in which internal forces or environment can be used to interact with the molecules. The adaptive algorithms uses the recursive divide and conquer approach to represent the molecular system. Haptic feedback was used for real time simulation and 432 degrees of freedom were activated. The whole molecule was manipulated like a rigid body but can be deformed by the simulation while interacting with other molecules. The forces applied by the simulation on the molecules are amplified in order to be felt by the user. The position scaling factor was carefully chosen in order to get trade-off between ease of manipulation and system stability. The proposed simulator has achieved high performance and gives idea how the internal forces are felt by user during simulation. The results of the simulator were compared with traditional interactive devices like mouse and joystick.

They also researched force control mechanism to connect molecular dynamic simulator and haptic devices instead of using traditional position control mechanism. The stability by changing the tuning parameter is compared for both force control and position control modes. The position control is sensitive to gain change while results were shown that force control with force feedback gave flexibility of changing parameters during the manipulation of molecular structure. The use of haptic devices helps to ease the analysis of nanostructure. They have used the SAMSON (System for Adaptive Modelling and Simulation of Nano-Objects) for the motion simulation of the structure. By adding direct force feedback stability has improved but transparency deteriorated.

Delalande et al. [38] have used low grain interactive molecular dynamics for exploration and hypothesis development of molecular interaction events. They have evaluated the feasibility of applications suitable for molecular assemblies having 1900 to over 300,000 particles. They have developed a free available software library MDDriver using protocols from VMD/NAMD for interactive molecular simulations. Their library offers a simple, modular and generic solution for combining co-ordinates

based calculation mode with various visualisation techniques. MDDriver was tested with visualisation tool (VMD) where molecular dynamic simulation was done in Gromacs and communication was done on TCP/IP protocol. In short, authors have developed a powerful tool which provides quicker and easy to manipulate framework for IMD.

Limet et al. [39] described the component based interactive dynamic visualisation applications. These applications are mainly composed of three components; simulation or data processing, visualisation and interaction parts which are required to be assembled precisely for interaction. They have proposed a framework Modulight which was implemented using MPI2 library which can handle well dynamic configurations and the optimised socket library OMQ as a communication layer. Modulight allows the user to create applications and components. The efficiency of the system is measured by the iteration frequency of visualisation and the framework results ware compared with FlowVR framework. Modulight was slower than FlowVR in the local deployment because FlowVR uses shared memory while in distributed environment the Modulight was faster than FlowVR. In both local and distributed environments, the Modulight results were stable than FlowVR.

Sasakura et al. [40] developed a system which uses mobile devices as input to manipulate the molecular structure in 3D visualisation environment. The dedicated 3D devices like 3D mouse, haptics devices or Wiimote for manipulating objects have their disadvantages and limitations. In this paper, they have used iOS device accelerometer in order to track the movements. The orientation of the device is detected by the X, Y and Z direction acceleration with respect to gravity. They have successfully tested the up/down, right/left and forward/backward movements using the iOS device and integrated with the visualisation system. They have developed a library by using these signals which can used to visualise the molecular reaction movements during

simulation. They have successfully recognises the signature of moving and leaning the device using the vibration signal. The shortfall of this method was the slow response when visualising in 3D environment which requires further work on improving response time. In addition to this, sometimes the system did not detect the intention of the user. This work is quite motivational for my current research project where I have overcome various gaps.

Sharma et al. [27, 41] developed a system 'Atomsviewer' in order to render billion atoms during molecular dynamics simulation. The Atomsviewer used the novel occlusion culling algorithm using probabilistic model which visualise the atoms based on the probability. Atomsviewer was run on distributed cluster of four computers in order to process the algorithms in parallel and dataset included one billion atoms. The system is composed of data extraction module which uses octree based hierarchical frustum culling algorithm to remove atoms outside frustum, probabilistic occlusion module which select the atoms with high probability using probability function, and rendering and visualisation module which uses the OpenGL graphics API. They have developed a GUI which gives the user flexibility to add rules and visualise results conforming those rules. They are developing a Neural Network base model in order to predict the user's next movement.

Meier et al. [42] presented a novel tool for interactive 3D visualisation and computational molecular simulations. The system has the data source and streaming server and a distributed viewer which may be located on local network or internet. The system provides the smooth animation of molecular simulation via stereoscopic options and interactive three dimensional navigation techniques. The system was tested on simple spherical particles and moderately complex molecular structures with various visualisation techniques efficiently. The proposed system can be applied in thermo physics research and computational fluid dynamics.

2.7 Summary

This chapter describes the application of haptic devices and other virtual reality systems for manipulating the molecular structures. Given the computational and graphical horsepower available with the latest hardware, the paradigm of current research has been shifting from 'how to represent' to 'what should be represented'. It is therefore fundamental to develop ways that would allow the users to interact with the visualised data dynamically. By integrating virtual environments in the complex simulations will help researchers explore details of reaction dynamics, manipulating objects during simulation, and advanced visualisation. In the last 5 years, as researchers, we have seen a revolution in the field of VR and 3-D visualization: costs dropped sensibly down while technological capabilities showed huge improvements, offering new opportunities for a wider range of users. Nowadays, it is not unusual to find 3-D monitors in a research lab or even more immersive and interactive systems, and this opens to a new interesting opportunity for working and managing scientific data. The haptic device provides the cost effective solution of tracking human gestures and therefore used in the research in order to interact with the molecular structure. Computer vision based approach of haptic device enables us writing algorithms to recognise the hand gestures which have ultimately provided the interaction with the simulation environment. The use of haptic device sensor will provide contactless sensing system which ultimately reduces the complexity of the simulation system. After having understood the existing limitations of the presently available devices, the new scheme of VAMDS was developed (presented in Chapter 4) to overcome the current limitations and to extend the applicability and accessibility of the current methods into a new regime.

Chapter 3 – Review and theory of MD simulation of contact loading

3.1 Concept, introduction and background

Molecular dynamics (MD) simulation in its current form is an integration of three disparate scientific disciplines namely, materials science, chemistry and computation. Though it exhibit statistical nature, but one can suitably study the properties of interest with high level of precision merely by applying Newton's second equation of motion to a system of atoms. This is shown schematically in figure 3-1 for the example of nanoindentation where the atoms within the substrate and the probe are at certain positions at time *t*. As the probe moves by a certain distance in time interval *Δt*, an atom *i*, acted on by the force F_{ij}, changes its position in the time interval *t+Δt*. Consequently, the new position of the atom *i* can be predicted using classical Newtonian mechanics.

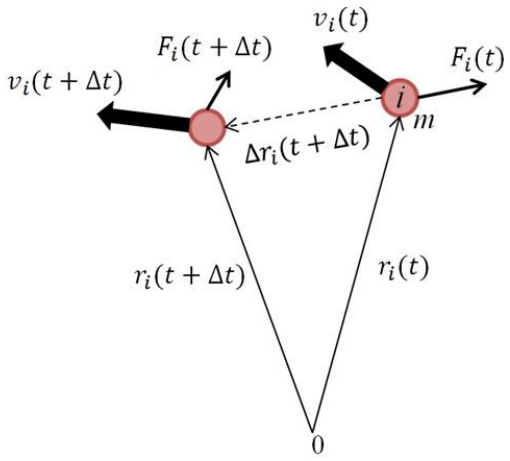

Figure 3-1: Principle of molecular dynamics simulation [43]

It was during the 1950s that Alder and Wainwright [44] applied MD to study the interactions of hard spheres in their pioneering work. Since then, the idea that Newton's second law of motion is valid even at the atomic scale has been used by enlarge for a multitude of scientific exploration to study the atomic systems. The basic principal of MD can be understood from the following equation:

$$m_i \frac{d^2 r_i}{dt^2} = F_i \qquad i = 1,2,....,n \tag{3-1}$$

where m_i is the mass of particle i and F_i is the force acting on it.

This equation can also be obtained from Lagrange's equation of motion which provides a more general framework for deriving equations of motion for systems of particles evolving under constraints.

3.2 Contribution of MD to the field of contact loading problems

It has been an important limitation of the experimental studies that they do not permit direct observation of all the events occurring at the atomic scale of time and length. An accurate understanding of the nano-tribological phenomena occurring at an atomic scale requires an insight into the energetic, structural, dynamic and rheological aspects of the system [45]. Understanding the relevant atomic level phenomena is the key to obtaining full knowledge of the atomistic mechanism of nano-indentation behaviour and this can be accomplished efficiently through the use of MD simulation [46, 47]. An example of how MD simulation permits *in-situ* monitoring of all the events occurring within a short time range such as transition of brittle failure to plastic deformation via ductile deformation in silicon [48] illustrated in figure 3-2.

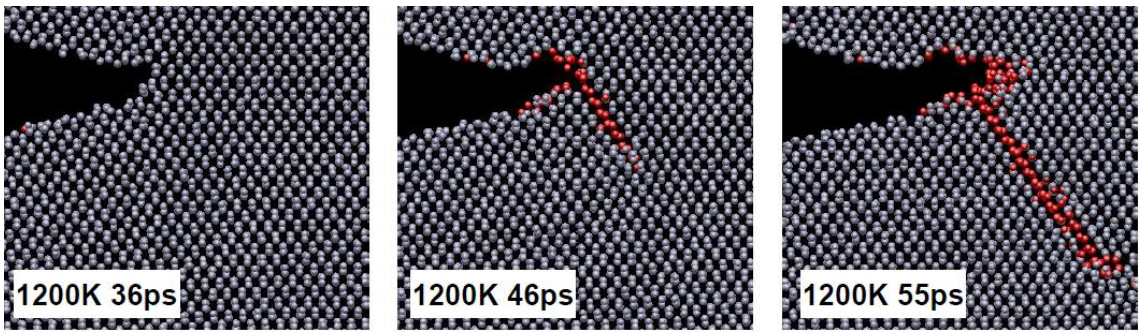

(a) Ductile failure *via* dislocation emission - Crack does not extend, but rather the lattice is sheared along the reddish region

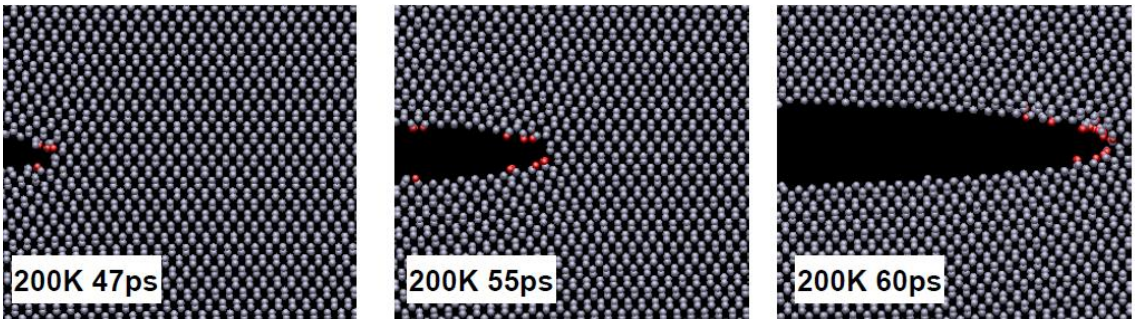

(b) Brittle cleavage failure – Crack extends suddenly and rapidly

Figure 3-2: Brittle-ductile transition in silicon as a result of change of temperature [48]

From figure 3-2a, it can be seen that ductile failure results from dislocation emission and the material gets sheared along a direction which is energetically more favourable than crack propagation. In contrast, during the brittle cleavage fracture, as shown in figure 3-2b, the crack extends suddenly and rapidly along its original direction. It is thus evident that MD is capable of providing insights into material failure mechanisms.

3.3 Potential energy function

MD simulation requires a constitutive description of the terms in which the atoms in a simulation interact. This interaction is governed by a potential energy function which approximately accounts for quantum interactions between electron shells and represents the physical properties of the atoms being simulated, such as its elastic constants and lattice parameters. While the newly developed formalisms are providing more accuracy, they are sometimes computationally very expensive as shown in figure 3-3.

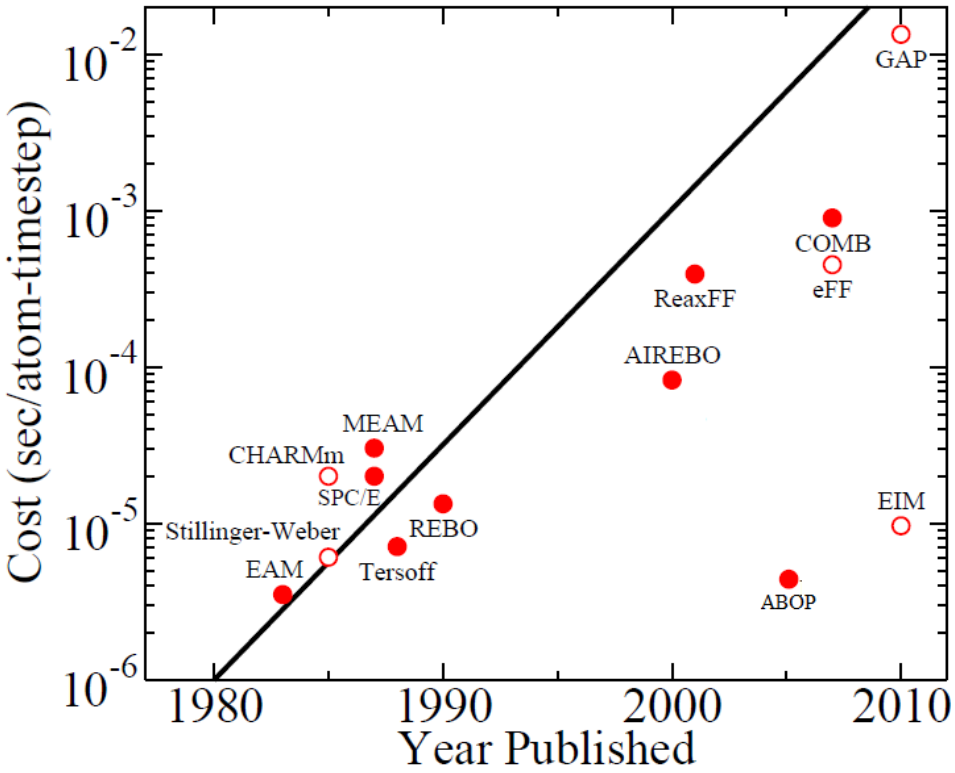

Figure 3-3: The increasing cost of processing power in seconds/atom/time step for state-of-the-art potential functions [49]

A nanoindentation simulation requires an interaction potential between the atoms of the indenter (carbon atoms) and the substrate. For example, from table 3-1 lists the parameters that can readily be used to carry out the nanoindentation of aluminium or copper using a diamond indenter.

Table 3-1: Morse potential for metallic systems [50]

Element	D (eV)	a ($Å^{-1}$)	r_0 (Å)
Cu-Cu	0.342	1.3588	2.866
Al-Al	0.2703	1.1646	3.253
C-C	3.68	2.2	1.54
Cu-C	0.087	1.7	2.05
Al-C	0.28	2.78	2.2

While Morse potential is a convenient potential, it fails to accurately predict the Cauchy pressure during contact loading which became a key motivation for the development of EAM potentials. However, covalent interactions in semi-conductive materials like silicon requires additional considerations and hence Tersoff potential was developed during the 1990s with the intention that it can dynamically allow the description of bond breaking and bond formation.

During its developmental phases, Tersoff proposed two variants for pure Si, wherein one variant Si(B) was found suited to study the surface properties of silicon while the other variant Si(C) was found more appropriate to study the elastic properties [51, 52] of silicon. Tersoff used the following mathematical description to describe covalent interactions in silicon:

$$E = \sum_i E_i = \frac{1}{2}\sum_{i \neq j} V_{ij} \tag{3-2}$$

$$V_{ij} = fc(r_{ij})[a_{ij} f_R(r_{ij}) + b_{ij} f_A(r_{ij})] \tag{3-3}$$

repulsive part $f_R(r) = A\exp^{(-\lambda_1 r)}$ 3-4

attractive part $f_A(r) = -B\exp^{(-\lambda_2 r)}$ 3-5

potential cutoff function as:

$$fc(r) = \begin{cases} 1 & r \leq R - D \\ \frac{1}{2} - \frac{1}{2}\sin\left(\frac{\pi}{2}\frac{(r-R)}{D}\right), & R - D < r < R + D \\ 0 & r \geq R + D \end{cases} \tag{3-6}$$

$$b_{ij} = (1 + \beta^n \zeta_{ij}^{\ n})^{-1/2n} \tag{3-7}$$

$$\zeta_{ij} = \sum_{k \neq i,j} fc(r_{ik}) g(\theta_{jik}) \exp(\lambda_3^{\ 3}(r_{ij} - r_{ik})^3 \tag{3-8}$$

$$g(\theta) = 1 + \frac{c^2}{d^2} - \frac{c^2}{[d^2 + (h - \cos\theta)^2]} \quad \text{3-9}$$

$$a_{ij} = (1 + \alpha^n \eta^n{}_{ij})^{-1/2n} \quad \text{3-10}$$

$$\eta_{ij} = \sum_{k \neq i,j} fc(r_{ik}) \exp[\lambda_3{}^3 (r_{ij} - r_{ik})^3] \quad \text{3-11}$$

In the above equations, r_{ij} is the distance between the atoms i and j, and θ_{jik} is the angle between bonds ij and ik A close examination of the above terms would also show that the potential also has angular dependence, but, since it is embedded inside the b_{ij} term, it does not give a fixed minimum angle between the bonds. Table 3-2 lists the parameters of this potential.

Table 3-2: Tersoff potential parameters for silicon [51, 52]

	Si(B)	Si(C)
A(eV)	3264.7	1830.8
B(eV)	95.373	471.18
λ_1(Å^{-1})	3.2394	2.4799
λ_2(Å^{-1})	1.3258	1.7322
A	0	0
B	0.33675	1.0999×10^{-6}
N	22.956	0.78734
C	4.8381	1.0039×10^{5}
D	2.0417	16.218
H	0	-0.59826
λ_3(Å^{-1})	1.3258	1.7322
R(Å)	3	2.85
D(Å)	0.2	0.15
Remarks	Suited for surface properties	Suited for elastic properties

In the subsequent years, Tersoff refined his formalism and proposed a few modifications to describe both Si and C along with their alloys. The new formalism took the following form:

$$E = \sum_i Ei = \frac{1}{2} \sum_{i \neq j} V_{ij}, \qquad V_{ij} = fc(r_{ij})[f_R(r_{ij}) + b_{ij} f_A(r_{ij})] \quad \text{3-12}$$

$$f_R(r_{ij}) = A_{ij} \exp(-\lambda_{ij} r_{ij}), \; f_A(r_{ij}) = -B_{ij} \exp(-\mu_{ij} r_{ij}) \quad \text{3-13}$$

$$fc(r_{ij}) = \begin{cases} 1 & r_{ij} < R_{ij} \\ \frac{1}{2} + \frac{1}{2}\cos[\pi \frac{r_{ij} - R_{ij}}{S_{ij} - R_{ij}}] & S_{ij} > r_{ij} > R_{ij} \\ 0 & r_{ij} > S_{ij} \end{cases} \quad 3\text{-}14$$

$$b_{ij} = \chi_{ij}(1 + \beta_i^{ni}\zeta_{ij}^{ni})^{-1/2n_i} \text{ , } \zeta_{ij} = \sum_{k \neq i,j} fc(r_{ik})\omega_{ik}g(\theta_{ijk}) \quad 3\text{-}15$$

$$g(\theta_{ijk}) = 1 + \frac{c_i^2}{d_i^2} - \frac{c_i^2}{[d_i^2 + h_i - \cos\theta_{ijk}]} \quad 3\text{-}16$$

V_{ij} describes the energy between two atoms (i and j), E_i is the the sub-function, (i, j, and k) are the three atoms in the system, f_R and f_A are the repulsive and attractive pair potentials, f_C represents a smooth cut-off function to limit the range of the potential etc. The mixing rule suggested by Tersoff for the two atomic species was as follows:

$$\lambda_{ij} = \frac{\lambda_i + \lambda_j}{2} \quad 3\text{-}17$$

$$\mu_{ij} = \frac{\mu_i + \mu_j}{2} \quad 3\text{-}18$$

$$A_{ij} = \sqrt{A_i A_j} \quad 3\text{-}19$$

$$B_{ij} = \sqrt{B_i B_j} \quad 3\text{-}20$$

$$R_{ij} = \sqrt{R_i R_j} \quad 3\text{-}21$$

$$S_{ij} = \sqrt{S_i S_j} \quad 3\text{-}22$$

Where χ_{ij} determines the attractive interactions between two atoms. The potential function parameters given by Tersoff for the refined function are tabulated in table 3-3.

Table 3-3 : Tersoff potential parameters for silicon and carbon alloys

	Year 1989 [53, 54]		Year 1990 [55]		Year 1994 [56]	
	Si-Si	C-C	Si-Si	C-C	Si-Si	C-C
A(eV)	1830.8	1393.6	1830.8	1544.8	1830.8	1544.8
B(eV)	471.18	346.74	471.18	389.63	471.18	389.63
$\lambda(Å^{-1})$	2.4799	3.4879	2.4799	3.4653	2.4799	3.4653
$\mu(Å^{-1})$	1.7322	2.2119	1.7322	2.3064	1.7322	2.3064
β	1.1×10^{-6}	1.5724×10^{-7}	1.1×10^{-6}	41.612×10^{-7}	1.1×10^{-6}	41.612×10^{-7}
n	0.78734	0.72751	0.78734	0.99054	0.78734	0.99054
c	100390	3804.9	100390	19981	100390	19981
d	16.217	4.3484	16.217	7.034	16.217	7.034
h	-0.59825	-0.57058	-0.59825	-0.33953	-0.59825	-0.33953
R(Å)	2.7	1.8	2.5	2.5	2.7	1.8
S(Å)	3	2.1	2.5	2.5	3	2.1
χC-Si	0.9776		0.9972		1.0086	

Since the Tersoff potential has been proposed, it has underwent a series of refinements yet has remained a basis for a sizeable amount of studies on silicon and carbon. The thing which Tersoff lacks most is the poor ability to describe the dimer properties of silicon such as the binding energy, D_0, the equilibrium bonding distance, r, the wave number, k, of the ground-state oscillation. In an attempt to address this shortcoming, another potential function, an analytical bond order potential (ABOP) was proposed [57]. ABOP takes the following form:

$$E = \sum_{i>j} f_c(r_{ij})[V_R(r_{ij}) - \underbrace{\frac{b_{ij} + b_{ji}}{2}}_{\bar{b}_{ij}} V_A(r_{ij})] \qquad 3\text{-}23$$

where *E*, the cohesive energy is described as the sum of individual bond energies with

the following expressions for repulsive and attractive contributions:

$$V_R(r) = \frac{D_0}{S-1}\exp\left[-\beta\sqrt{2S}(r-r_0)\right] \quad 3\text{-}24$$

$$V_A(r) = \frac{SD_0}{S-1}\exp\left[-\beta\sqrt{2/S}(r-r_0)\right] \quad 3\text{-}25$$

D_0 and r_0 are the dimer energy and bond length.

The cutoff function in the ABOP potential is given by:

$$f_c(r) = \begin{cases} 1 & r < R-D \\ 0 & r > R+D \\ \frac{1}{2} - \frac{1}{2}\sin\left(\frac{\pi}{2}\frac{r-R}{D}\right) & |R-r| \le D \end{cases} \quad 3\text{-}26$$

where the parameters R and D specify the position and the width of the cutoff region. The bond order is given by:

$$b_{ij} = \left(1+\chi_{ij}\right)^{-1/2} \quad 3\text{-}27$$

$$\chi_{ij} = \sum_{k(\neq i,j)} f_c(r_{ik})\exp[2\mu(r_{ij}-r_{ik})g(\theta_{ijk}) \quad 3\text{-}28$$

and the angular function is given by:

$$g(\theta) = \lambda\left(1+\frac{c^2}{d_2} - \frac{c^2}{d^2+(h+\cos\theta)^2}\right) \quad 3\text{-}29$$

The parameters of the potential energy function for carbon and silicon and their interactions in the ABOP formalism are shown in table 3-4.

Table 3-4: Potential function parameters of silicon and carbon [58]

	Si-Si	C-C	Si-C
D_0 (eV)	3.24	6	4.36
r_0 (Å)	2.222	1.4276	1.79
S	1.57	2.167	1.847
β (Å^{-1})	1.476	2.0099	1.6991
Γ	0.09253	0.11233	0.011877
C	1.13681	181.910	273987
D	0.63397	6.28433	180.314
H	0.335	0.5556	0.68

2μ ($Å^{-1}$)	0	0	0
R (Å)	2.9	2	2.4
D (Å)	0.15	0.15	0.2

However, whether its Tersoff or ABOP potential, they both have a major limitation in that they assume a theoretical scheme for determining the next-nearest neighbour atoms and to avoid computational time, they both work on a narrow distant-dependent cutoff scheme. It has however been recently shown that such a consideration results in an undesirable change in the energy-distance relation leading to enforcing the bond-breaking requiring higher forces than actual. It is this assumption that limits the applicability of either Tersoff or ABOP to study brittle behaviour and hence a more improved version of scheme has recently been proposed that improves the way how the cutoff scheme on bond order potentials is estimated. By doing so, the improved potential (screening function) is able to more accurately. produce close results with experiments [59]. This was achieved by decoupling the condition for a nearest-neighbour relationship from the range of the potential [60]. The anecdote of this improvement is that the screening functions increases the range of Tersoff and ABOP potentials thereby makes them long range potentials [61]. It suggests that the potential energy function is an important consideration for a realistic MD simulation. There are some shortcomings of the currently used potential functions. For example, the ductile-brittle transition in silicon cannot be described well by the ABOP or BOP (Tersoff potential energy function). In this regard, Pastewka *et al.* [62] have highlighted key considerations needed to use a potential energy function to model wear phenomena.

3.4 Preparations for the MD simulation

A schematic diagram of the nanoindentation simulation model used in this work is shown in figure 3-4. In figure 3-4, the atoms in the indenter were kept fixed (diamond indenter was assumed to be an infinite rigid body structure) and in the three test cases,

the crystal orientation of silicon was varied. Goel *et al.* [63] have provided a glance of other research works where a higher velocity (up to 500 m/s) has been frequently used to overcome the limitations of MD simulation. To achieve more realistic results, we made use of an indentation velocity of 20 m/s as has been recently used on HPC systems [64]. Also, we made use of long range Tersoff potential energy function [61] for describing silicon and carbon as it provides improved description of silicon.

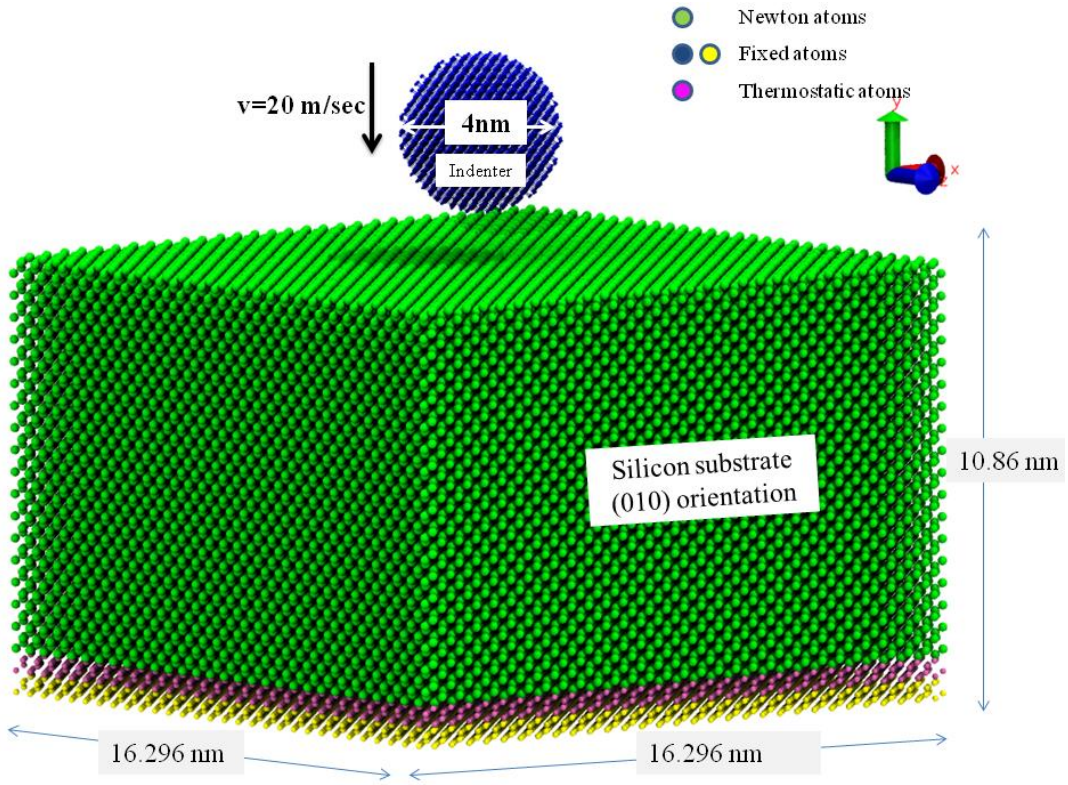

Figure 3-4: Schematic of MD simulation model

As evident in the literature, the atoms in the model are divided into three different zones: Newton atoms, thermostatic atoms and boundary atoms. The purpose of having the boundary atoms is to anchor the workpiece at its location during the simulation. In a nanoindentation process, the environment will serve the purpose of heat carrier but the MD simulation model is extremely small and therefore an artificial thermostatic region is manually created mimic a heat sink. Consequently, the temperature of the thermostatic atoms is re-scaled to a 300K at each step of the computation.

MD simulations are performed within a simulation box size L which have N number of atoms. To build a large enough model, it is usually needed to implement a periodic boundary condition (PBC). To use PBC in a simulation of *N* atoms confined to a volume *Vn*, we imagine that *Vn* is only a small portion of the bulk material, called the primary cell, where the bulk is considered to be composed of the primary cell surrounded by replicas called image cells. The image cells are of the same size and shape as the primary cell, each containing *N* atoms, themselves images of the atoms in the primary cell as illustrated schematically in figure 3-5.

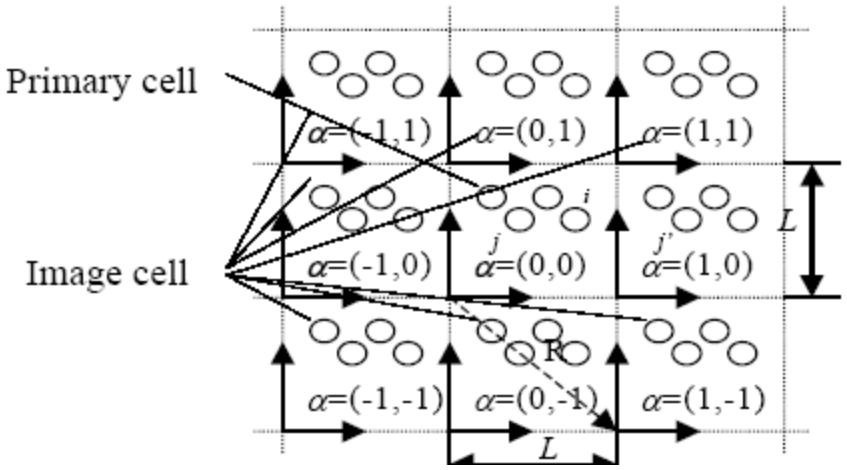

Figure 3-5: Periodic boundary condition [65]

Silicon and diamond have different lattice constants and hence, care is needed in using a PBC involving these two different kind of materials. Basically, the length of the PBC must be so chosen that the lattice constants of diamond and silicon are in integer proportion e.g. $L_z = n_1 \times a_1 = n_2 \times a_2$ where L_z is the cell size,n_1 and n_2 are integers and a_1 and a_2 are the lattice constants of diamond and silicon respectively. Theinitial configuration of atoms is constructed by assigning the atoms to coordinate of a lattice (figure 3-6a), which can be done by energy minimization and the velocities to the atoms are assigned using Maxwell-Boltzmann distribution.

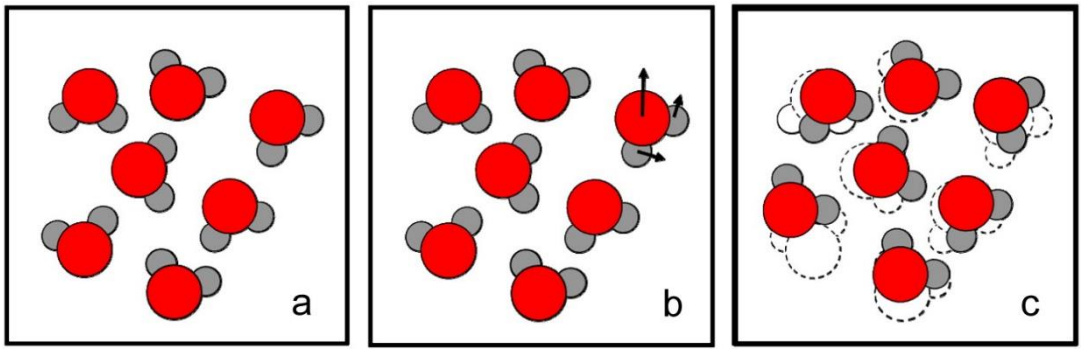

Figure 3-6: Illustration of MD (a) The initial positions of the molecules are specified (b) Force on each atom due to the other atoms in its neighbourhood is calculated. (c) Potential energy function predict the newer positions and velocities of the atoms at a specified time [66]

After minimization, the velocity of all the atoms was scaled to 300K using the process of equilibration. During equilibration, the energy of the system attempt to stabilise and thus it fluctuates until saturation (figure 3-6b). Once the system achieve steady state, the velocity scaling is removed and the system follows LAMMPS NVE dynamics (figure 3-6c). It is in this particular step that the proposed VAMDS system provides an exclusive capability of having more control on the simulation process. As evident from the above, one of the major problems in performing MD simulations is achieving the local state and its transition to a new (desired) equilibrium state which is a rare event. The users making use of VAMDS can direct the simulation institutively to faster convergence to find desirable/feasible state of to study the mechanism of chemical reaction to enable more clear and precise understanding of the atomic events.

3.5 Post processing of results

3.5.1 High pressure phase transition in silicon like materials

Mechanical deformation involves a number of processes occurring simultaneously i.e. movement of dislocations, brittle fracture, tribochemistry and phase transformation of the material. Of all these mechanisms, the phase transformation of brittle materials under high surface pressures is of particular interest as this opens up the possibility of

obtaining a ductile response from brittle materials [67]. Atomic trajectories contains complex position/coordinates of atoms and sometimes, it is extremely daunting to clearly discriminate definite phases of materials. It may therefore require combining several methods to analyse material's microstructure In this regard, the review of Stukowski [68] provides a good insight into the application of most of these methods which have been by enlarge already implemented in OVITO (an open source code) Some of these methods are briefly discussed below.

3.5.1.1 Coordination number

Silicon has been an extensively researched material. Across other research works, the work of Cheong *et al.* [69] suggested Si-I to Si-II phase transformation in silicon based on a global radial distribution function showing changes in the bond length of silicon atoms from 2.35 Å to 2.43 Å and 2.58 Å, respectively. Other researchers have used a criterion of coordination number which would suggest that the above change in inter-atomic distance is associated with a change in the coordination number of silicon from 4 to 6 [70]. In our work, same criterion was used for its relative ease of implementation in LAMMPS.

3.5.1.2 Radial distribution function

The radial distribution functions (RDF) are helpful plots to monitor the peaks or the distances between adjacent neighbouring atoms. As shown in figure 3-7, a central atom (blue colour) remains the point of focus from which the neighbour distance of an atom (green colour) is measured as the first neighbour distance atoms across several atoms(white colour). Mathematically, RDF, $g(r)$, gives the number of atoms $dn(r)$ at a distance between r and $r + dr$ from a given atom and is mathematically expressed as follows:

$$dn(r) = \frac{N}{V} g(r) 4\pi r^2 dr \qquad 3\text{-}30$$

where V is the model volume, N represents total number of atoms, V and $g(r)$ is the radial distribution function.

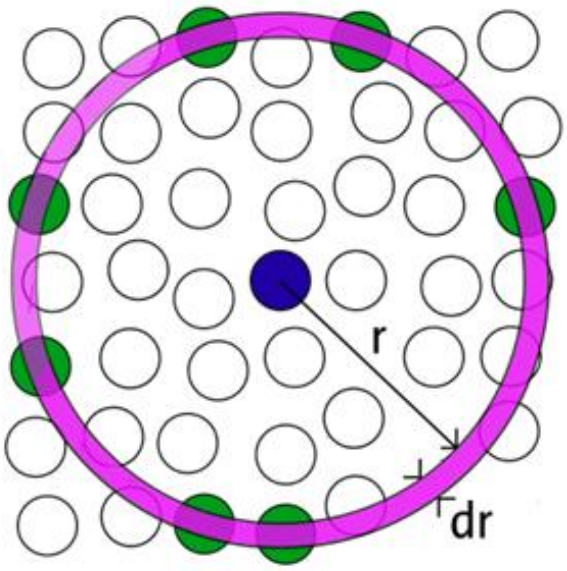

Figure 3-7: Schematic diagram of radial distribution function [71]

3.5.2 Calculation of stresses

The stress tensor for an atom i can be calculated from equation 3-31.

$$S_{ab} = -\left[\begin{array}{l} mv_a v_b + \frac{1}{2}\sum_{n=1}^{Np}(r1_a F1_b + r2_a F2_b) + \frac{1}{2}\sum_{n=1}^{Nb}(r1_a F1_b + r2_a F2_b) + \\ \frac{1}{3}\sum_{n=1}^{Na}(r1_a F1_b + r2_a F2_b + r3_a F3_b) + \frac{1}{4}\sum_{n=1}^{Nd}(r1_a F1_b + r2_a F2_b + r3_a F3_b + r4_a F4_b) \\ + \frac{1}{4}\sum_{n=1}^{Ni}(r1_a F1_b + r2_a F2_b + r3_a F3_b + r4_a F4_b) + \sum_{n=1}^{Nf} ri_a Fi_b \end{array} \right] \qquad 3\text{-}31$$

where a and b denote x,y,z to generate the 6 components of the symmetric stress tensor. LAMMPS readily offers a command compute stress/atom which makes use of the equation shown in 3-31. It was used to obtain the stress tensor for each atom for a region of volume V during the simulation. The total stress acting on that volume of region V was divided by V in order to obtain the physical stress tensor. Thus obtained,

the physical stress tensor was converted into equivalent von Mises stress. von Mises stress (corresponding to maximum deviatoric strain energy) measure is a well-defined and established criterion to predict yielding in solid material and this von Mises stress (σ_{vonmis}) was computed using the following equation:

$$\sigma_{\text{von Mises}} = \sqrt{\frac{(\sigma_{xx}-\sigma_{yy})^2+(\sigma_{yy}-\sigma_{zz})^2+(\sigma_{zz}-\sigma_{xx})^2+6(\sigma_{xy}^2+\sigma_{yz}^2+\sigma_{zx}^2)}{2}} \quad 3\text{-}32$$

It may be noted that the volume of an atom fluctuates during the process of deformation and this is why an elemental atomic volume was considered for the computation of the stress tensor. The total stresses acting on that element were computed and were divided by the pre-calculated total volume of that element.

3.5.3 Calculation of the temperature in the indentation zone

At the moment, there is no direct way to measure the temperature of an MD system. There are indirect ways to measure the temperature such as conversion of kinetic energy of the atoms into the equivalent temperature. However, it may be recalled that the kinetic energy of a system is an ensemble property and keeps fluctuating. So one must average out the kinetic energy of a group of atoms to indirectly arrive at the average values of the temperature of the system. This was accomplished using the relationship between kinetic energy and temperature as follows:

$$\frac{1}{2}\sum_i m_i v_i^{\,2} = \frac{3}{2} N k_b T \quad 3\text{-}33$$

where N is the number of atoms, v_i represents the velocity of i^{th} atom, k_b is the Boltzmann constant (1.3806503×10^{-23} J/K) and T represents the calculated temperature. During the nanoindentation process, the instantaneous fluctuations in kinetic energy/atom were high so these were averaged over few timesteps before arriving at an equivalent temperature.

3.6 Summary

This chapter has provided a detailed description of the molecular dynamics simulation. Starting with an introduction to the concept and the background to its development, it goes on to provide the basis of the calculations required to perform an MD simulation of the nanoindentation process. This chapter also justifies the choice of the potential energy function to perform an appropriate simulation. It was recognized that most of the previous research is done using a Morse potential function which is more appropriate for diatomic molecules than for hard, brittle materials which are covalent. The strong need for an appropriate potential function was highlighted and a critical review of this type of formalism has been presented. Taking the example of the brittle-ductile transition, it has also been shown that it was only through molecular dynamics simulations that a conceptual understanding of this phenomenon is gathered.

It is also noted that, in order to replicate simulation results or to perform other simulations, the simulation conditions need to be understood very well. Accordingly, the preparations required for a simulation and the post-processing tools are also comprehensively described, including measurement of cutting forces using the three-body potential function, use of a periodic boundary condition and measurement of stresses during a simulation.

Chapter 4 – Vision-augmented molecular dynamics simulation

4.1 Introduction

MD simulation is a scientific algorithm through which an assemblage of atoms and/or molecules is given prescribed intermolecular interactions for a specified period of time to yield a trajectory of their movement. As discussed in the previous chapters, the idea to bring the comfort of performing MD simulation more intuitively, can be realised by bringing the use of haptic devices in the simulation framework and to achieve this, a new method being referred as "Vision-augmented Molecular Dynamics Simulation" (VAMDS) was developed in this work. The idea evolved from the use of the hardware that has been recently used on such research endeavours i.e. Microsoft Kinect that can suitably capture the human gestures. The gestures are eventually transformed into commands, which are sent to the visualization software Jmol for changing the positions or orientation of different atoms within the molecule. The whole process takes place on-line in a dynamic way and hence it offers more flexibility than any of the previous proposed technique. The Jmol in turn write the molecular script coordinates based on the visual inputs and creates an atomic coordinated file automatically which is then fed to an engine like LAMMPS for performing the simulation. This chapter aims at presenting all the design aspects of the proposed VAMDS system.

4.2 Generic scheme of performing vision-augmented MD

The proposed system is presented in figure 4-1 and figure 4-2. As shown in the two aforementioned figures, there are three distinct components of this system: the Gesture Application (Gesture App), the Jmol visualizer and the OVITO. OVITO was mainly used for the transformation of the 3-D coordinates of atoms to write them in a specific mode of data file which are compatible to perform the MD. Larger Atomic/Molecular

Massively Parallel Simulator (LAMMPS) is currently at its pinnacle with respect to the number of users interested in carrying out molecular dynamic simulations. The team at Sandia laboratories [72] has by now provided all the capabilities to LAMMPS to enable the simulation on parallel processors. In this research, LAMMPS was used to perform the atomic simulations by providing the inputs generated from the haptic device and thereby avoiding writing the complicated scripts. One of the recent advancement in the area of computer vision has been the creation of a revolutionary device called Kinect that can be used and manipulated in different areas. This device is able to control PC computers and laptops via hand gestures without using markers (mouse & keyboard). GestureApp and the Jmol visualizer are interconnected through TCP/IP protocol (see dotted lines in figure 4-1). The Gesture App is responsible for detecting human gestures, converting them into Jmol commands and then sending them over TCP/IP to Jmol server. The commands captured by the haptic device concerning modified atomic positions are sent to the visualization software e.g. (Jmol, OVITO etc.) using gestures recognition. Algorithms were written which in turn helps to obtain a description of a newer geometry with modified positions or orientations of the atoms. The modified file is saved in a location which is then fed to the Molecular Dynamics Simulator LAMMPS for performing the simulation with revised inputs. In addition, OVITO also provides visualisation of the final simulation results that come from the simulator LAMMPS. In the subsequent sections of this chapter, first a step-by-step functional description of the whole system has been given. In the next section, a detailed internal working of the Gesture App has been provided followed by brief introduction of the Jmol Visualizer along with the necessary commands that were used for manipulation of the molecules. The last section describes the scripting framework that glues all the modules within the Vision-Augmented Molecular Dynamics Simulator shown in Figure 4-1 and figure 4-2.

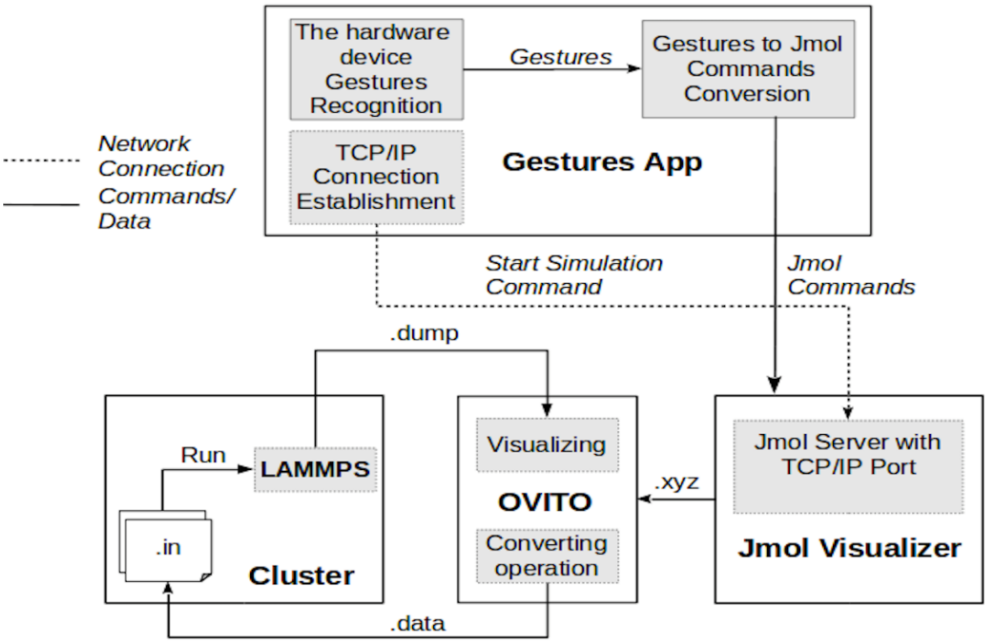

Figure 4-1: Vision-Augmented Molecular Dynamics Simulation

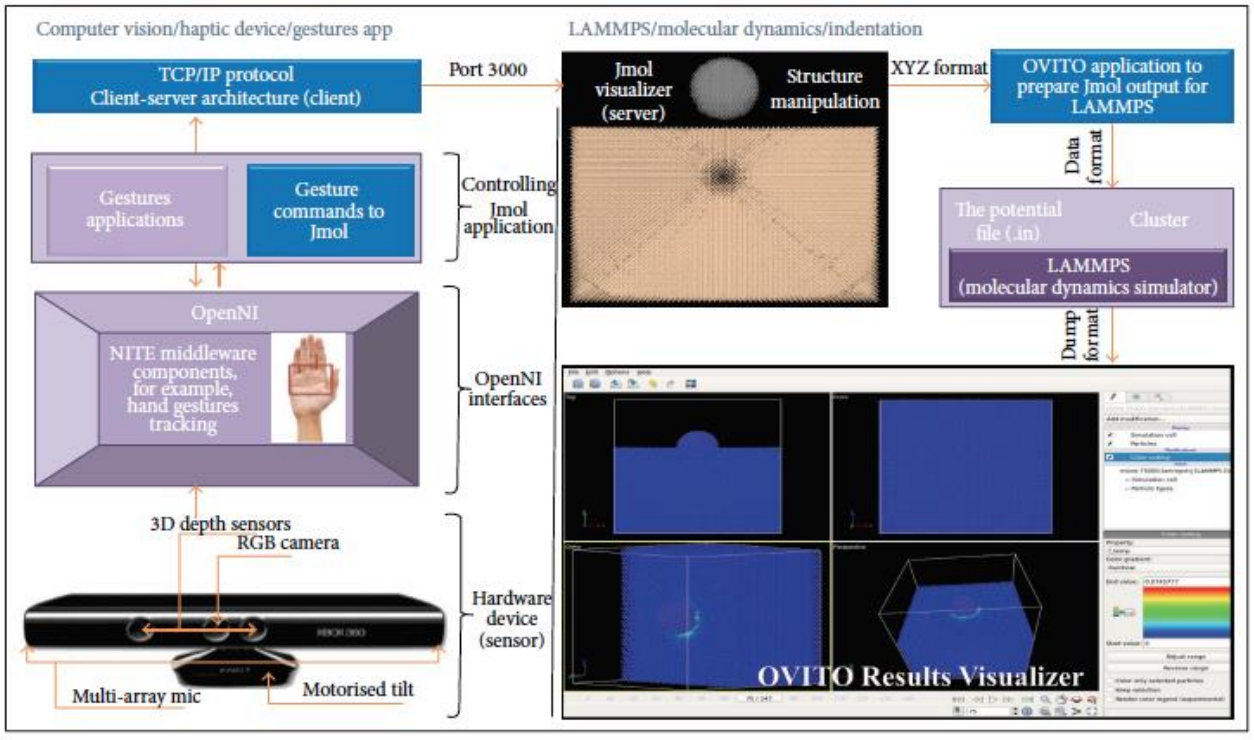

Figure 4-2: The integration between Computer vision and Molecular Dynamics Simulation

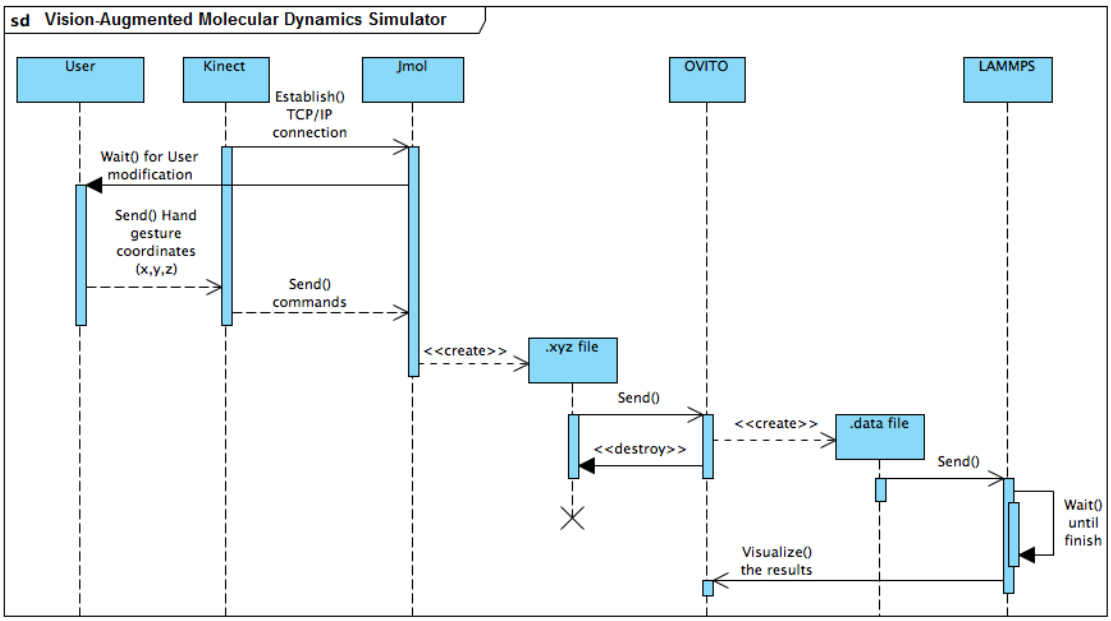

Figure 4-3: Sequence diagram for VAMDS

In figure 4-3, a sequence diagram shows, as parallel vertical lines (lifelines), different processes or objects that live simultaneously, and, as horizontal arrows, the messages exchanged between them, in the order in which they occur. This allows the specification of simple runtime scenarios in a graphical manner. Typically these are associated with use case realizations in the Logical View of the system under development. Solid arrow heads represent synchronous calls, open arrow heads represent asynchronous messages, and dashed lines represent reply messages.

4.3 Functional Descriptions

The vision-augmented molecular dynamics simulation comprises various steps that are shown below.

- **Step 1:** Start the Gesture App, the Jmol Visualizer and the OVITO application. The connection is established between the Gesture App and the Jmol Visualizer.
- **Step 2:** Load a file contains molecular structure in xyz format. For example, SiliconIndentation.xyz in the Jmol Visualizer.
- **Step 3:** Initiate the Gesture App by using the Wave gesture.
- **Step 4:** Manipulate the molecular structure. For example, changing the position

of different atoms within the molecular structure using different gestures

- **Step 5:** Save the new molecular structure in a new xyz file using the Circle gesture. This also sends the output from Jmol to OVITO.
- **Step 6:** The OVITO performs necessary format conversion (convert the modified file from xyz format to LAMMPS data format) then sends the converted file to cluster to run the LAMMPS simulator. The results are then displayed in OVITO window.

4.4 The Gesture App

The Gesture App is used to detect gestures using the Microsoft Kinect. The Microsoft Kinect is a multi-sensor device, which is primarily used for extracting depth information from the scene and for gesture recognition. A typical Microsoft Kinect device is shown in Figure 4-3.

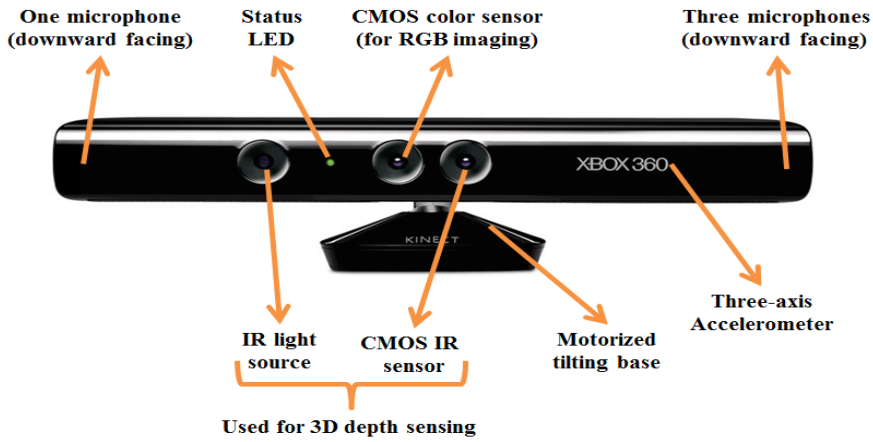

Figure 4-4: Microsoft Kinect

By the means of Kinect, inferring body position is a two-stage process (i) compute a depth map and (ii) infer body position. In stage (i), the depth map is constructed by analysing a speckle pattern of infrared laser light. This technique of analysing a known pattern is called as structured light. Hence, Kinect uses infrared laser light with a speckle pattern while making use of a random decision forest. Eventually, the Kinect combines structured light with two classic computer vision techniques: depth from

focus, and depth from stereo (parallax). For this reason, the Microsoft Kinect contains an Infrared (IR) light source and a CMOS IR sensor, an RGB camera, an accelerometer and a microphone array. The IR light source and the CMOS IR sensor are used for gesture recognition. A lot of libraries have been developed for this sensor, which provides depth information and gesture recognition. A major limitation of the Kinect is that only offers handling one sensor at a time i.e. one hand movement at a time, however, this work seeks to overcome this limitation by capture the movement of right as well as the left hand and this has been explained in the next section. Also, in this work, we have used a layered framework to extract gesture information. Starting from the bottom, we have the OpenNI layer. It interacts with the sensor's device as well as the middleware components like the NITE module which implements gesture recognition, scene analysis and skeleton tracking. The second layer is the NITE algorithms which uses computer vision techniques for extracting information from raw depth data. The third layer is the NITE controls, an application framework that provides functions for gesture recognition and User Interface (UI) controls to enable application developers to follow the flow according with the information, event and action generated by the NITE module. The layer at the top is the application itself that receives callbacks from the NITE controls or interacts directly with OpenNI to have access to the data generated by the raw sensor. Using the raw sensor data, the framework shown in Figure 4-4 provides a fixed set of gestures. These include wave, circle, swipe left, swipe right, swipe up, swipe down and push gestures. An example gesture like the wave gesture is shown in Figure 4-5.

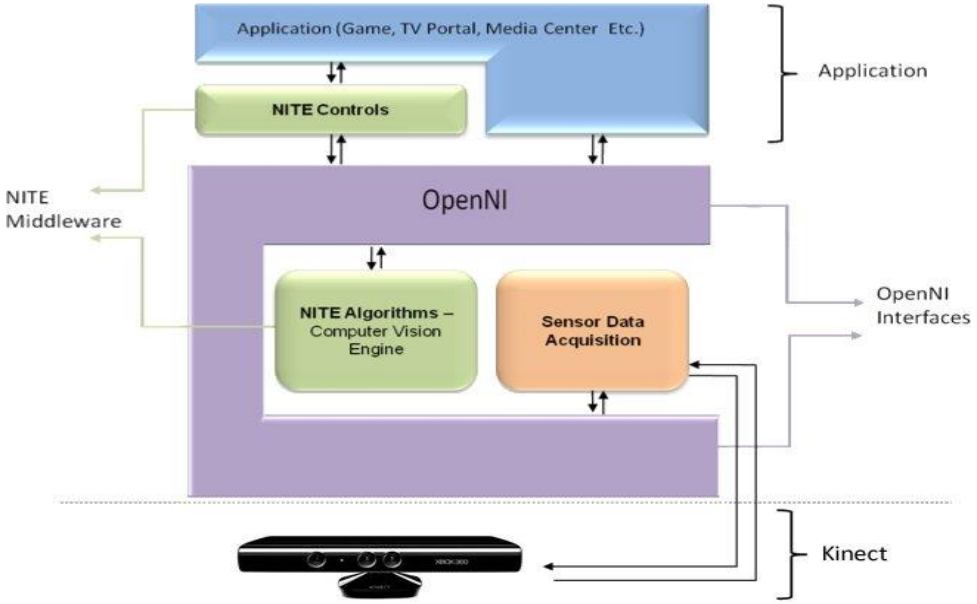

Figure 4-5: OpenNI and NITE Framework for Gesture Recognition [2]

In addition to the individual gestures, OpenNI provides skeleton tracking as well. However, there are certain limitations with the framework. For example, the OpenNI-based framework provides gesture information from only one hand (right or left), whereas we intend to control the simulation using gestures from both hands. We take the Simple Control application from the NITE and make the following modifications.

- Detect all the gestures coming from the NITE algorithms for a single hand, which is right hand in our case.
- Control the mouse cursor within the Linux environment using the right hand movement.
- Detect the gestures using a customized algorithm for the left hand.
- Control the second mouse cursor within the Linux environment using the left hand movement.
- Establish connection-using TCP/IP with the JMOL server.
- Convert the gestures into JMOL commands.
- Send the JMOL commands to the JMOL server.

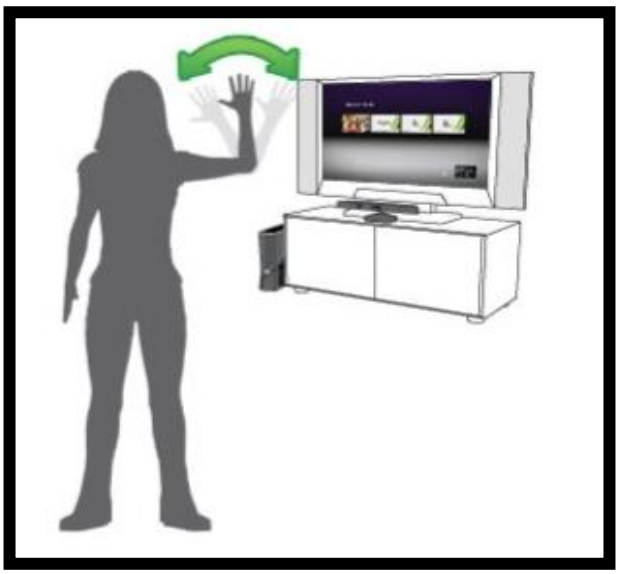

Figure 4-6: Wave Gesture [1]

4.4.1 Gestures Detection Using NITE Algorithms

As mentioned before, there are judiciously chosen gestures which are supported by the NITE algorithms. In the main function of the Gesture App, the gestures are initialized and their callbacks are gestured, a sample of it is shown below:

Sample Code Snippet:

```
XnVWaveDetector wc;
wc.RegisterWave(NULL, OnWaveCB);
wc.RegisterPointUpdate(NULL, OnPointUpdate);
pSessionGenerator->AddListener(&wc);
```

The above-mentioned code performs two operations: a XnWaveDetector object is declared for the wave gesture and a callback function OnWaveCB is registered. Whenever a user performs the wave gesture as shown in Figure 4-5, the callback is called and necessary action can be specified for this particular gesture. We similarly declare detectors for other gestures along with the registration of their callbacks.

4.4.2 Mouse Control using Right Hand Movement

A desired feature of the Gesture App is to provide mouse control using the Kinect sensor. If we analyze the above mentioned code snippet, along with the callback OnWaveCB for the wave gesture, another callback OnPointUpdate is also registered.

This callback is called whenever there is any movement in our right hand. The 3D coordinates from the Kinect sensor tracks the position of the right hand and these are passed into the callback function. These 3D coordinates are transformed into 2D screen coordinates. A mouse cursor is then positioned on these 2D screen coordinates. Additionally, we apply a very simple low pass filter to smooth out the jerky mouse movements.

4.4.3 Customized Algorithm for Left Hand Gestures Detection

As mentioned earlier, the OpenNI-based framework provides gesture information from only one hand, which is the right hand in our case. However, both hands are tracked by this framework and their coordinates are passed to the OnPointUpdate callback function. Based on the hand ID, we choose whether to use NITE algorithms or custom algorithm as shown in Figure 4-6(a). We find out the coordinates for a particular hand using the hand ID. Once we have the 3D coordinates for the left hand, then we apply customized algorithm to extract gestures as shown in Figure 4-6.

The algorithm calculates the change in the movement of the hand in all three axes. This movement is represented by the vector [Δx, Δy, Δz]. Using a heuristic approach, we then detect various gestures based on the dominant movement along a particular axis. As an example, a SwipeLeft gesture is detected by having a movement in the -x direction i.e. Δx is less than zero. We, therefore, check whether Δx is greater than both Δy and Δz and also greater than a particular threshold. Similarly, we detect Steady, SwipeRight, SwipeUp, SwipeDown and Push gesture by applying a different heuristic.

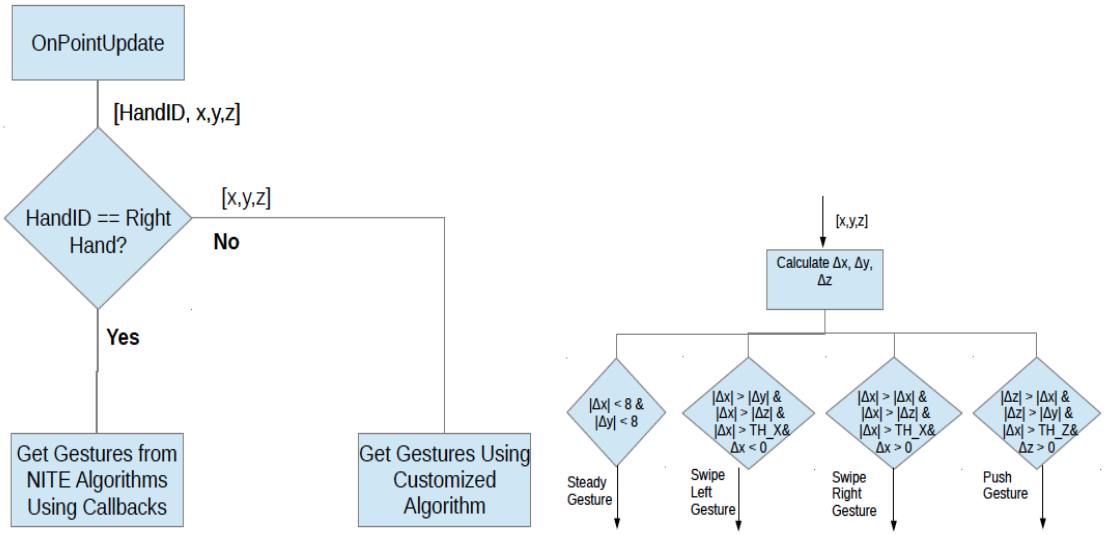

(a) Algorithm Selection (b) Custom Algorithm for Left Hand Gestures Detection

Figure 4-7: Gestures Recognition (Only Steady, SwipeLeft, SwipeRight and Push Gestures are shown for the Left Hand)

4.4.4 Mouse Control using Left Hand Movement

In order to use both hands for manipulation of the molecules within the JMOL Visualizer, we created a virtual mouse device by issuing the following command within the Linux shell.

```
sudo xinput create-master new
```

We get the mouse ID for the newly created virtual mouse and attach left hand movements with this mouse cursor. This is all done automatically in our framework.

4.4.5 Connection with the JMOL Visualizer and Gesture App

The Gesture App is responsible for detecting gestures, mapping them to specific JMOL commands and sending them to the JMOL server. It also triggers the simulation by detecting a special gesture. In order to achieve all this, we need the Gesture App to communicate with the JMOL Visualizer. We have chosen TCP/IP protocol for communication between these two modules. Although, currently these two modules are running on the local host but they can be made to run on different computing nodes by using the TCP/IP protocol. This communication setup is shown in Figure 4-7.

The scheme of client-server communication along with the respective port numbers are shown in Figure 4-7 that were used for establishing connections between Gesture App and the Jmol Visualizer.

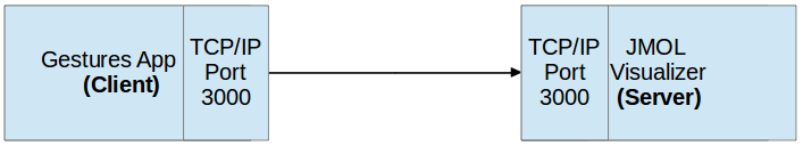

Figure 4-8: Communication between the GestureApp and other modules.

4.4.6 Gestures to JMOL Command Conversion

Since we intend to manipulate the position of atoms merely using gestures, we need to convert the gestures into appropriate JMOL commands. Some of these conversions are tabulated in Table 4-1. In order to send the JMOL command to the JMOL Visualizer, we use a Wireshark tool to capture the data on TCP/IP port to identify the exact structure of the command. As an example, in order to send the command zoom in, we need to execute movement Swipe left (left hand) and Swipe right (right hand) in front of haptic device. Gesture application will convert this to the Jmol command format which is “zoom in” and send it to Jmol server via TCP/IP port to do the operation “zoom in” to the molecular structure visualised on Jmol.

We prepare this string for each command and send it over TCP/IP to the JMOL Visualizer. Once the string is received by the JMOL server, it executes a particular command and the respective action is taken accordingly. As an example, in the above case, the loaded molecule gets zoomed in. For other commands, we just replace the zoom in field with the corresponding JMOL command.

Table 4-1: Gestures to JMOL Command Mapping

S/No.	Hand Gestures	Jmol commands
1	Push (right hand)	Left mouse button click
2	Swipe right (right hand)	Right button mouse click
3	Swipe left (right hand)	Set picking drag molecule
4	Swipe up (right hand)	Set picking drag atom
5	Swipe down (right hand)	Set picking drag bond
6	Swipe right (left hand) and Swipe left (right hand)	Zoom out
7	Swipe left (left hand) and Swipe right (right hand)	Zoom in
8	Swipe up (left hand)	Set picking delete atom
9	Swipe down (left hand)	Set picking delete bond
10	Push (left hand)	Spin on/off
11	Circle (right hand)	Write the output from Jmol in XYZ format and send this to OVITO

4.5 The Jmol Visualizer

Jmol is an open-source Java viewer for chemical structures in 3D [73] that does not require 3D acceleration plugins. Jmol [74, 75] returns a 3D representation of a molecule that may be used as a teaching tool, or for research e.g. in molecular dynamics, chemistry and biochemistry [76].

Jmol is a powerful tool that has a lot of features and abilities. For example as shown in Table 4-1, Jmol has the ability of allowing the users to manipulate the molecular structures on the screen. Furthermore, one of the Jmol features that Jmol contains console, which allow the user to integrate it with other applications via TCP/IP protocol. A popular feature is an applet that can be integrated into web pages to display molecules in a variety of ways. For example, molecules can be displayed as "ball and stick" models, "space filling" models, "ribbon" models, etc. Jmol supports a wide range of molecular file formats [77], including Protein Data Bank (pdb), Crystallographic Information File (cif), MDL Molfile (mol), and Chemical Markup Language (CML).

4.6 Open Visualisation tool (OVITO)

The OVITO application is another key module of this framework [68, 78-81]. After the

molecular manipulation process is completed in the JMOL Visualizer, a new coordinate file is written which triggers the conversion process. The Gesture App module detects the circle gesture from the right hand and sends the output as xyz file from Jmol. OVITO receives the modified file in xyz format from Jmol then performs necessary format conversion to prepare the main structure for LAMMPS simulator (OVITO converts the modified file from xyz format to LAMMPS data format).

4.7 Scripting Framework

In order to launch all these different applications namely the Gesture App, the JMOL Visualizer, OVITO and LAMMPS, a scripting framework was built within the Linux shell (See Appendices at the end). A hierarchy of different scripts is shown in Figure 4-8. It all starts with the MainScript.sh script. This script runs two main processes, the initiation of looping process that manages, transmits, and sends commands. The RunMultipleScript.sh, launches Gesture App, JMOL Visualizer and also creates a virtual mouse device, which is attached with the left hand movement. Once the JMOL Visualizer is launched, it loads the molecule and the gestures are then detected using the Gesture App, which are converted to the JMOL commands. The commands are used to manipulate the molecular structure. Once the manipulation process is done and an output file is generated, a conversion command within the MainScript.sh is sent to OVITO. OVITO is capable of performing format conversions that are necessary in order to make the LAMMPS simulator work. Once the conversions are done successfully, the LAMMPS simulator is launched which then provides the output of the simulation. The final output files are then visualized using OVITO.

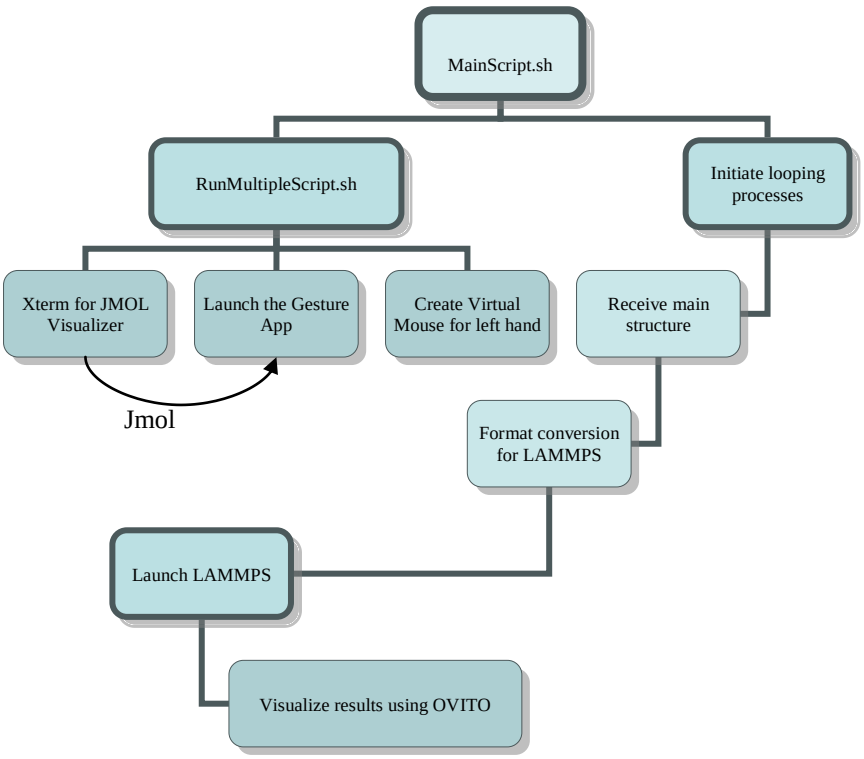

Figure 4-9: Scripting Framework

4.8 Summary

In order to perform the so called "Vision-augmented Molecular Dynamics Simulation" (VAMDS) this chapter has provided a detailed description of the hardware and the software systems involved in this research. In the beginning a generic scheme has been provided that comprehensively summarises the three distinct systems of the proposed system and they were: Gesture Application (Gesture App), the Jmol visualised and the OVITO. Eventually the system basically help convert the human gestures into programmable commands, which are then sent to the visualization software like Jmol for changing the positions or orientation of different atoms within the molecule. The modified file is then sent to a Molecular Dynamics Simulator like LAMMPS for performing the actual simulation. Following this generic scheme a detailed description of each application, their command line, the hardware system and the software used such as the OVITO and their respective communication protocol with each component has also been provided.

Chapter 5- VAMDS results for the nanoindentation of silicon

5.1 Introduction

One of the key advantages of using VAMDS in the current investigation was to perform the nanoindentation and this can well be extended to other contact loading processes as well. In particular, VAMDS readily allows varying the indentation depth merely by hand movements and this can hence readily be used to understand indentation size effects. However, there are still some technical problems which were not examined in the current investigation through MD. This is because either they are too complex to be investigated through MD or it is very time-consuming and costly to cover these problems using the MD simulation. Some of these processes yet to be examined are exploration of the brittle-ductile transition and high temperature indentation behaviour of silicon. This chapter highlights some of the nanoindentation trials performed using the MD simulation using the vision-augmented MD simulation method. In particular, a case study was undertaken on nanoindentation trial of silicon substrate on the (010), (110) and (111) orientation using a rigid diamond indenter described by a long ranged Tersoff potential function (screening functions applied to Tersoff potential function). As highlighted earlier, the study of anisotropy using VAMDS become more convenient since the microstructure of the material can be changed easily merely by the use of hand-gestures and was hence a more amenable problem for the case study performed here.

5.2 VAMDS results on single crystal silicon

5.2.1 Methodology of VAMDS of nanoindentation of silicon

As explained in the earlier chapters, the entire process was automated so that the HPC server can call the LAMMPS engine to generate the simulation output in the form of a trajectory at the desired time steps. The output files obtained from LAMMPS were

programmed to save in the local computer from the HPC server and the process continues until the whole directory containing the LAMMPS output is copied to the local computer. This cycle continue while in the meantime, OVITO interactively make the use visualise each file copied from the HPC server to the local computer. VAMDS

The aim of the study was to explore the crystal anisotropy of silicon in such a way that the orientation of the crystal can be switched merely by the hand gestures. To this end, the simulation model was first developed by following the standard algorithm, boundary conditions and ensemble in the same way as has been previously done in other research papers [63, 82, 83]. A schematic simulation model used to carry out the simulation is shown in figure 5-1. In figure 5-1, the atoms in the indenter were kept fixed (diamond indenter was assumed to be an infinite rigid body structure) and in the three test cases, the crystal orientation of silicon was varied. Goel *et al.* [63] have provided a glance of other research works where a higher velocity (up to 500 m/s) has been frequently used to overcome the limitations of MD simulation. To achieve more realistic results, we made use of an indentation velocity of 20 m/s as has been recently used on HPC systems [64]. Also, we made use of long range Tersoff potential energy function [61] for describing silicon and carbon as it provides improved description of silicon.

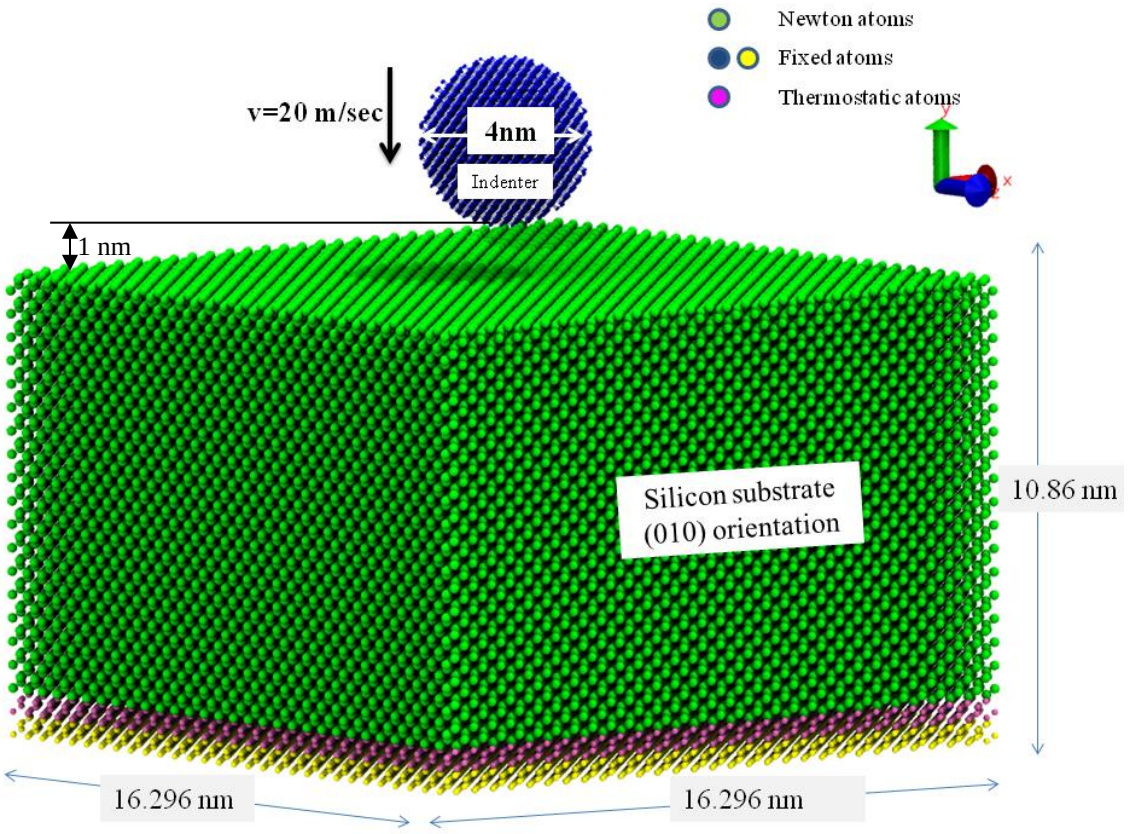

Figure 5-1: Schematic of the MD simulation model of silicon

The details of the parameters used to develop the MD simulation model are shown in Table 5-1. In the MD simulation model, to avoid any artificial effect of the temperature (due to thermal fluctuations and thermal vibrations), a low temperature of 10K was used to equilibrate the sample and perform the nanoindentation. During the MD simulation, the atomic stress tensor was calculated by considering an elemental atomic volume (1nm × 1nm × 1nm = 68 atoms) of silicon in the deformation zone right underneath the indenter.

Table 5-1: Details used for the development of MD simulation model

Dimensions of the silicon workpiece	Crystal orientation of silicon	Number of atoms
16.296 nm × 10.864 nm ×16.296 nm	(010)	144,000
15.9667 nm × 10.7548 nm × 15.9667 nm	(110)	137,088
15.9667 nm × 11.29 nm × 16.132 nm	(111)	145,152
Equilibrium lattice constants	Silicon : 5.432 Å and Diamond : 3.5656 Å	
Indenter and specimen surface distance	1 nm	
Depth of indentation	2 nm	
Speed of indentation and retraction	20 m/s = 0.02 nm/ps	
Diameter of the indenter	4 nm	
Boundary conditions	Periodic in X and Z direction	
Potential function used	Screening bond order Tersoff potential function [61]	

In addition to stress calculation, further analysis was carried out by estimating the contact pressure (p_m) underneath the indenter. Contact pressure (p_m) is defined as the ratio of the instantaneous normal force (F) on the indenter and the projected area (A) which is calculated as ($2\pi \times a \times h$) for a spherical indenter where $a = \sqrt{h(2R-h)}$ is the contact radius of the spherical indenter, R is the radius of the indenter and h is the instantaneous displacement of the indenter. The average value of the contact pressure (after it attains saturation value) is also referred to as nanoindentation hardness (H) of the material.

A popular way of calculation of the elastic modulus (Es) and hardness (H) of the material from the load-displacement (*P-h)* plot was proposed by Oliver and Pharr [84] during the last decade of 20^{th} century. Their method relies on calculation of the

projected contact area by drawing an imaginary line, typically following the power law, on the top 1/3rd part along the unloading curve of the *P-h* plot. The slope of this curve (S) thus enables to obtain the reduced elastic modulus of the material which can then be used to obtain Es (elastic modulus) of the specimen using the following equations:

$$E_r = \frac{1}{\beta}\frac{\sqrt{\pi}}{2}\frac{S}{\sqrt{A}} \qquad 5\text{-}1$$

$$\frac{1-\upsilon_s^{\,2}}{E_s} = \frac{1}{E_r} - \frac{1-\upsilon_i^{\,2}}{E_i} \qquad 5\text{-}2$$

In equation (5-1) and (5-2), E_r is the reduced elastic modulus (N/m^2), S is the slope of the top 1/3rd part of the unloading curve which were obtained as 729 N/m (for 010 oriented Si), 820 N/m (for 110 oriented Si) and 914 N/m (for 111 oriented Si) from the simulation results, β=1 a constant for spherical indenter, A is the Projected area (m^2) which varies with the depth of indentation. For accuracy of computation of E, other parameters such as υ_s =0.3459 (Poisson's ratio of silicon), υ_i =0.103 (Poisson's ratio of Diamond), E_i = 1056.48 GPa (Young's modulus of diamond) were obtained directly from the potential function.

5.2.2 Calibration of the VAMDS system for nanoindentation of silicon

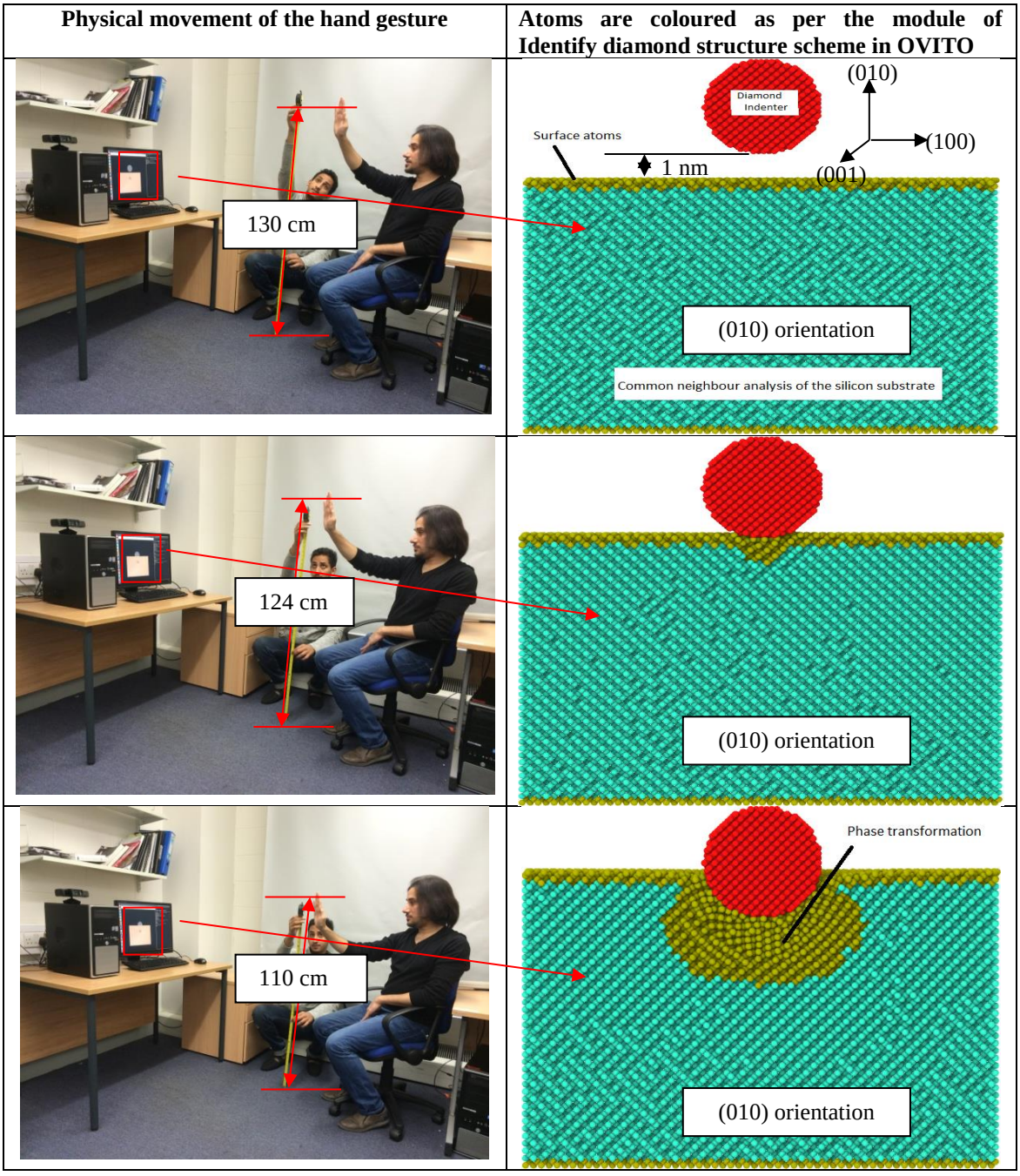

Figure 5-2: Comparison of physical movement with the movement in the MD simulation model (a) at the beginning of the simulation, (b) when the indenter establishes contact with the substrate and (c) final indentation depth was achieved.

Figure 5-2 shows the progressive physical movement of the human hand sensed by the gesture application (left column) and transformation of this physical hand movement into the corresponding displacement of the indenter into the substrate (right hand column). The physical distances of the hand movements were captured through a measurement tape and were compared with the movement of the indenter in the MD

simulation model so calibrate the system (transferability of the hand movement into the equivalent displacement of the indenter). The relation between these two movements was plotted and is shown in figure 5-3. Knowing this relation was a preliminary step for calibrating the newly proposed VAMDS system.

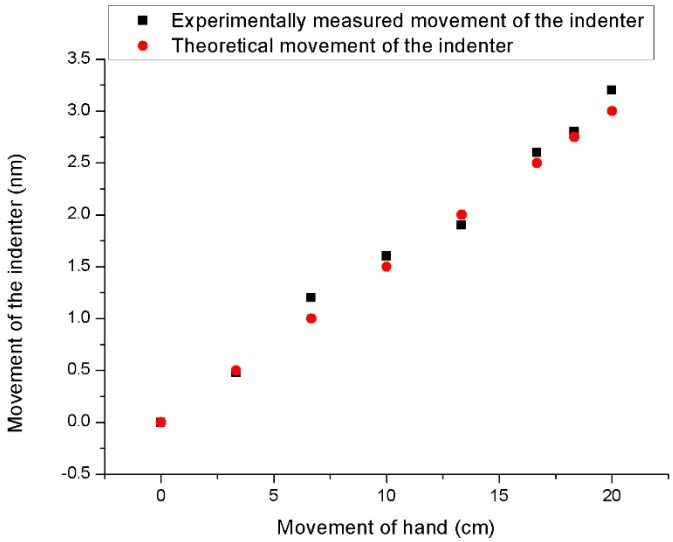

Figure 5-3: Relationship between physical movement of hand gesture and indenter in the MD model

5.2.3 VAMDS results on nanoindentation of silicon

The ductile behaviour of brittle materials is often attributed to an event recognized as high-pressure phase transformation (HPPT). HPPT enforces brittle materials to become ductile for the short duration of loading which upon unloading eventually transforms to amorphous phase of the brittle material. HPPT of silicon during its nanoindentation has been explained to be driven from the deviatoric stress rather than temperature [63] in the deformation zone. Much of the literature on silicon nanoindentation, have reported HPPT to be the primary mechanism governing the plasticity of silicon that causes brittle-ductile transition. There is however a noticeable exception of Mylvaganam *et al.* [85] observed nanotwinning (associated with Si-I to bct-5 phase transformation) in silicon along the <110> direction that stops at Shockley partial dislocation. It was therefore relevant to assert the occurrence of HPPT in this work for which an indicator

known as coordination number was used which has been recursively used in the literature to study structural phase transformation in silicon [47].

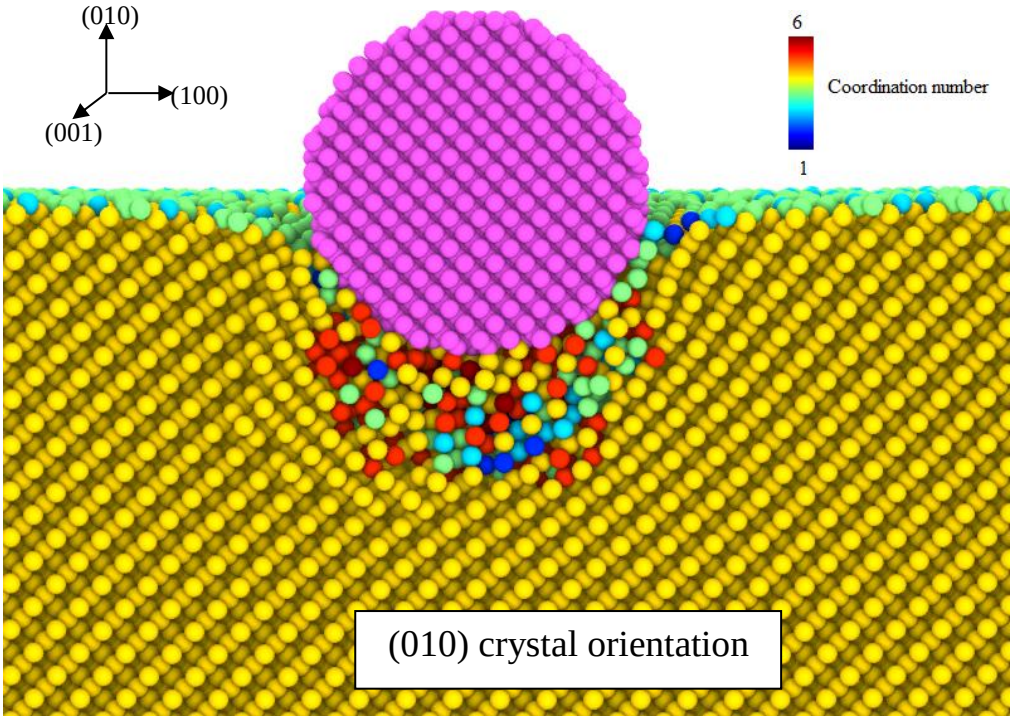

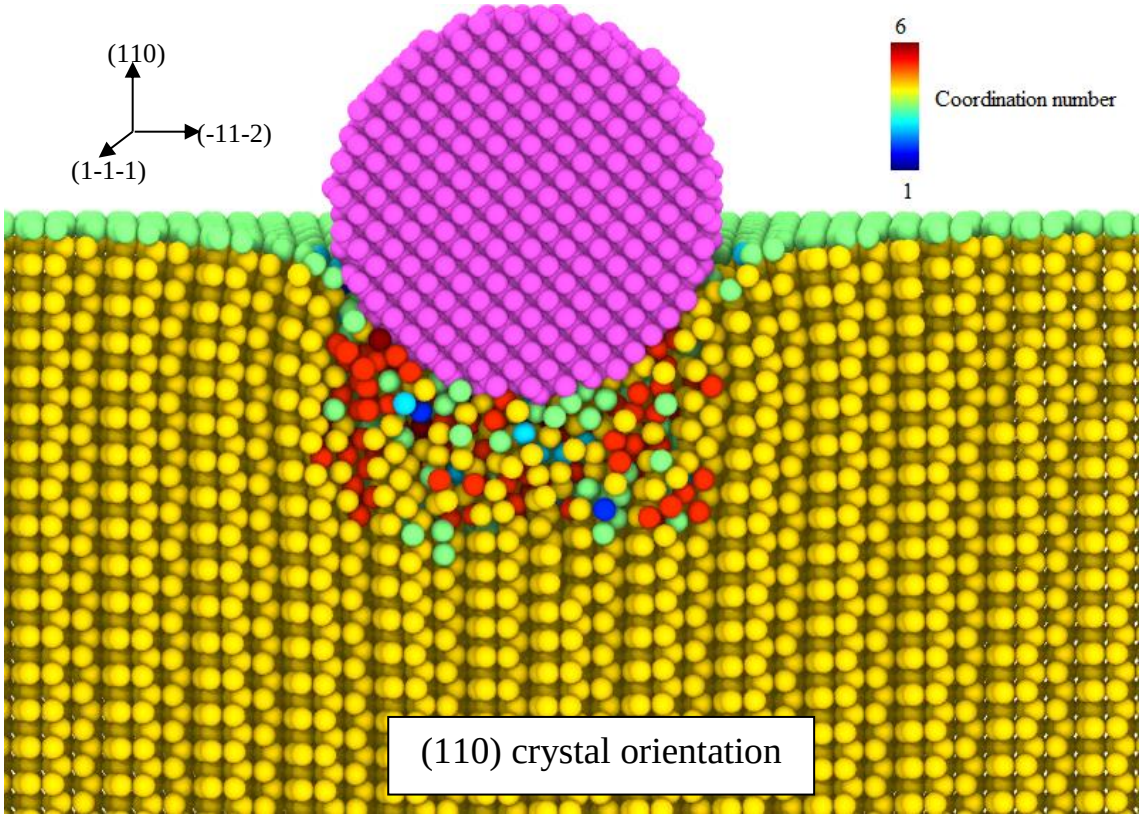

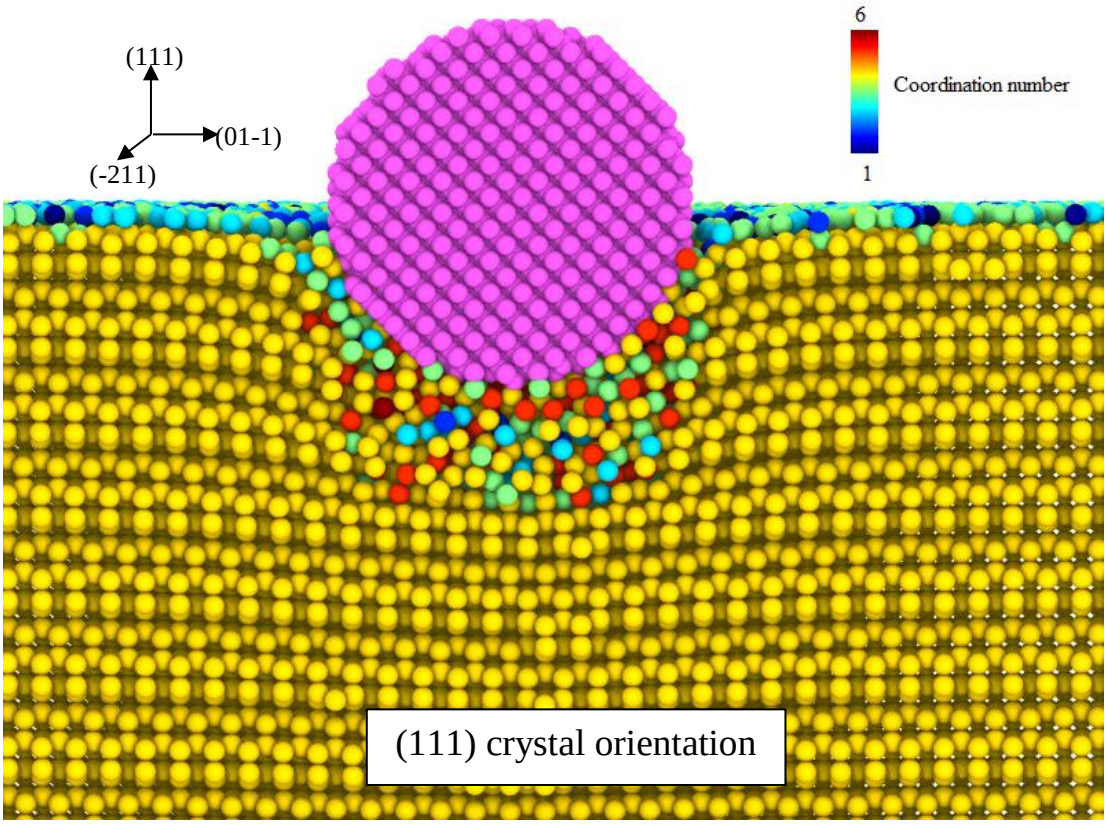

Figure 5-4: Cross-sectional view of the silicon substrate in the XY plane highlighting the change in coordination number at peak indentation depth of 2 nm on three orientations

A snapshot from the MD simulation showing the change in coordination number during peak loading of silicon on various orientations is shown in figure 5-4. The coordination number of 4 (figure 5-4) is representative of bulk silicon while coordination number of 1 and 2 on the free surface of silicon substrate represents the dangling bonds on the Si-terminated nascent surface. During the nanoindentation, the coordination number in the indentation zone was observed to change from 4 to 6 with a corresponding change in the number of nearest neighbour atoms suggesting the occurrence of amorphisation. Most of the this was observed to occur along the <110> direction, which is the recognized widely as the direction of slip plane in silicon [86].

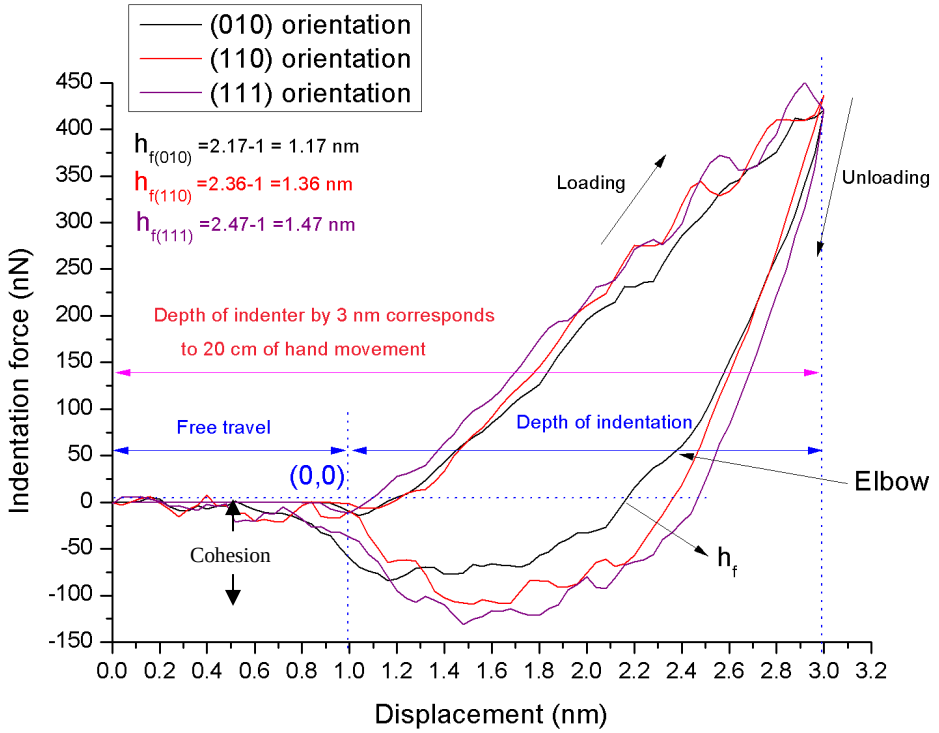

Figure 5-5: P-h plots of the nanoindentation for all three crystal orientations of silicon

Figure 5-5 is a *P-h* plot obtained from the velocity (displacement) controlled nanoindentation simulation where the penetration depth of the diamond tool was kept fixed at 2 nm. An interesting observation concerning the *P-h* plot comes from the work of Jang *et al.* [87] where a good correlation between unloading curve and the phase of the material formed post-indentation of silicon was observed. Based on the micro-Raman spectra, the authors proposed that the unloading discontinuity, often called as 'pop-out', corresponds to the formation of metastable Si-XII/Si-III crystalline phases, while the hysteresis, called the 'elbow' is associated with the formation of a-Si. In figure 5-5, an interesting feature observed from the P-h plot was that the unloading curve for the (110) and the (111) substrate followed power law whereas the unloading curve on the (010) substrate showed an elbow. This characteristic is a testimony to the formation of a-Si upon the retraction of the indenter on the (010) orientation.

Another interesting feature observed from the *P-h* plot obtained from the MD simulation was the residual indentation depth (h_f) that can also be used to characterize

the recovery of the indented surface upon retraction of the indenter. In this case, h_f was quantified from the P-h plot (figure 5-5) for all the three simulated orientations and was found inevitably different in all the cases i.e. h_f (010) was minimum while h_f for the (111) orientation was maximum whereas h_f(110) was intermittent. This suggests that at atomic scale, the (010) orientation will show higher extent of elastic recovery than the (111) orientation of silicon. This result is somewhat consistent with the earlier work of Shibata *et al.* [88] where a Schmidt-type slip orientation factor was proposed and the $\langle 1\bar{1}0 \rangle$ direction either on the (100) or on the (111) planes was recognized as more preferred combination to plastically deform the silicon. Lastly, beside a monotonic increase in the loading curve, a strong cohesion between the indenter and the substrate during retraction was also observed. HPPT is highly direction sensitive [89, 90] i.e. pressure or hydrostatic stress required for transformation on the (111) orientation is lower than that required to induce the transformation on the (100) orientation [86]. Literature suggest that the transformation pressure required to cause metallisation of silicon varies between 9-18 GPa [91]. It may however be noted that the hydrostatic pressure differs from deviatoric stress [92]. During nanoindentation, silicon undergoes both shear as well as compression making it different from the case of simple compressive pressure.

Table 5-2: Computational results obtained from the nanoindentation simulation

Silicon	(010) orientation	(110) orientation	(111) orientation
Average hardness (GPa) at indent depth of 2 nm	16.99	18.22	18.48
Elastic modulus (GPa) at indent depth of 2 nm	129	147	167
h_f/h_{max} (Extent of elastic recovery)	1.17/2 = 0.585	1.36/2 =0.68	1.47/2 =0.735
Peak maximum Von Mises stress in the indent zone (GPa)	11.07	22.75	16.72
Peak maximum Tresca stress in the indent zone (GPa)	5.91	12.11	9.14
Peak maximum octahedral shear stress in the indent zone (GPa)	5.21	10.72	7.88
Peak hydrostatic stress in the indent zone (GPa)	20.11	21.98	16.62
Peak temperature in the indentation zone (K)	300	419	438
Features of the P-h curve during unloading	Elbow formation corresponding to a-Si formation	No feature	No feature

As it can be seen from table 5-2, the hydrostatic stress (pressure) [93] in the indentation zone was observed to be maximum on the (110) orientation followed by (010)

orientation and it was minimum for the (111) orientation. This correlation was however not the same for the von Mises stress and Tresca stress in the indentation zone.

For the two kind of deviatoric stresses, the (110) orientation showed maximum values whereas the (010) orientation showed least value. The peak average temperature in the indentation zone was rather high, especially considering the fact that nanoindentation process was carried out at 10 K. At its peak, the (111) orientation showed the maximum temperature of about 438 K followed by the (110) orientation at 419 K whereas the (010) orientation showed the least temperature of 300 K. Finally, the elastic modulus was obtained from P-h plot using Oliver and Pharr method and accordingly the variation in E and hardness on all the three crystal surfaces with respect to change in the indentation depth is plotted and shown in figure 5-6.

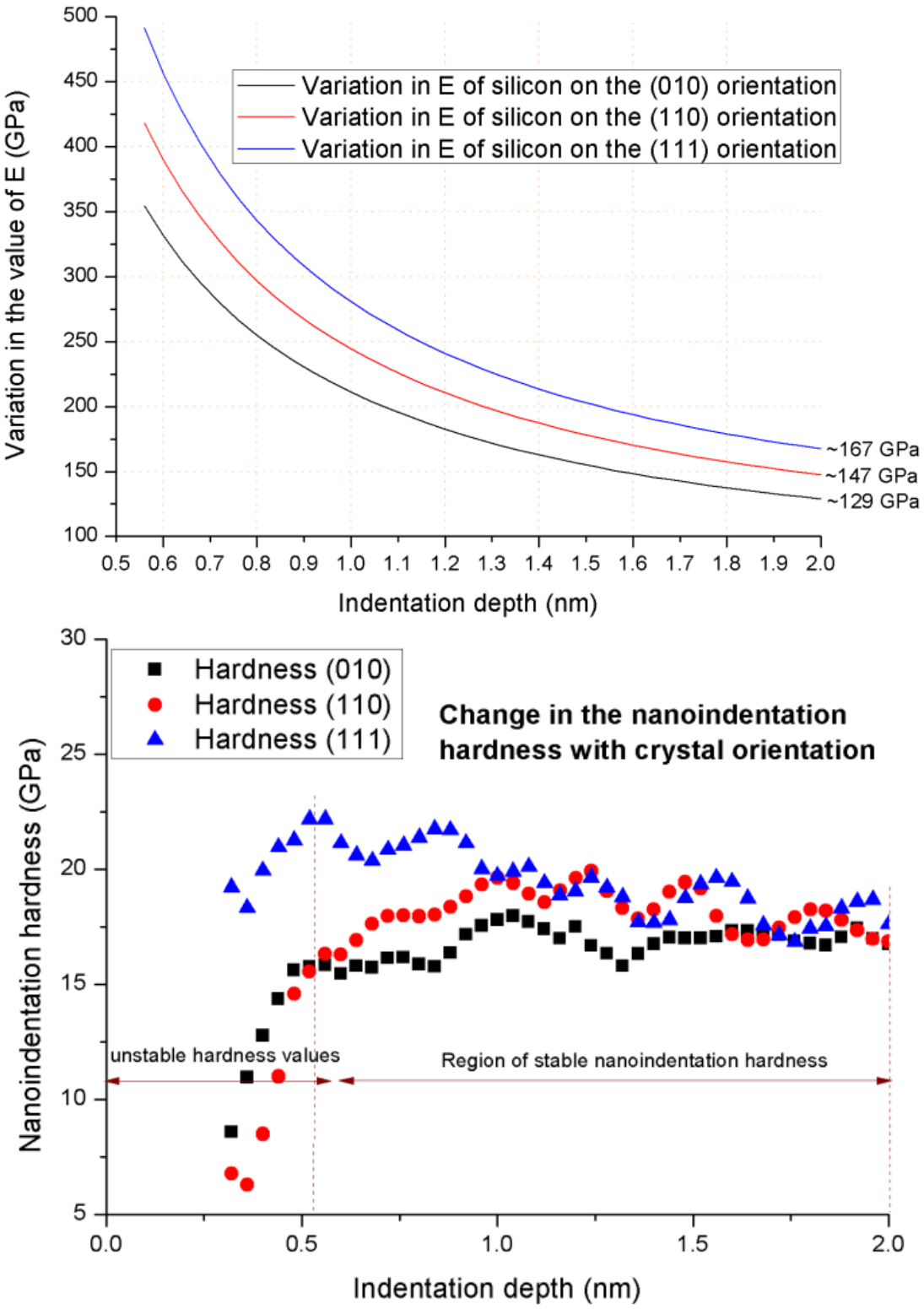

Figure 5-6: Variation in the (a) elastic modulus and (b) nanoindentation hardness of silicon with respect to the indentation depth

It is interesting to note from figure 5-6a that the elastic modulus at finite indentation depth of few nanometres decrease sharply until attaining a saturated value as the indentation depth increases. At an indentation depth of 2 nm, the elastic modulus of the

three simulated orientations was obtained as 129 GPa for the (010) orientation, 147 GPa for the (110) orientation and 167 GPa for the (111) orientation. These values are well comparable with the experimental values of the elastic modulus of silicon [57, 94] and resembles similar to what has been obtained from MD [95].

5.3 Summary

This chapter presents the simulation results of nanoindentation of silicon obtained by VAMDS. With what had been somewhat a cumbersome process to do via a traditional scripting process, VAMDS facilitate the shuffling of crystal orientation and to achieve any given indentation depth merely by the hand movements swiftly. The results obtained from the testbed study can be summarized as follows:

1. Obtaining the variation in the hardness and elastic modulus using classical way of doing molecular dynamics simulation would have been a relatively tedious task but with the implementation of the VAMDS, this is easily achievable. The use of haptic device as shown in this work reduces the pain of obtaining mechanical property *via* P-h profile as the simulation run can be restarted from any point merely by the use of hand gestures which is thus the merit of this work.
2. At an indentation depth of 2 nm, it was seen that the unloading curve for the (110) and the (111) substrate follows power law whereas the unloading curve on the (010) substrate showed an elbow which was found related with the formation of a-Si upon the retraction of the indenter on the (010) orientation only. Furthermore, the elastic constants of silicon obtained from the nanoindentation varied in the order of $E_{111} > E_{110} > E_{010}$.
3. The mechanism of ductility in silicon occurs due to the high pressure phase transformation (HPPT) that is driven by stress rather than temperature. For

HPPT to occur in silicon, the (110) orientation requires maximum hydrostatic stress (pressure) and (111) orientation requires minimum hydrostatic stress while the (010) orientation requires an intermittent value. However, this index changes when the stress state becomes deviatoric e.g. during nanoindentation the von Mises and Tresca stress for the (110) orientation were found maximum while the (010) orientation showed least value whereas the (111) orientation showed somewhat an intermittent value.

Chapter 6- VAMDS results for the nanoindentation of tantalum

6.1 Introduction

Unlike previous chapter, this chapter provide the nanoindentation simulation results of a metallic material known as Tantalum (Ta), primarily to extend the applicability of the proposed VAMDS on the metallic systems. Some of these processes that were not studied in this work but well doable with ease using the proposed VAMDS system is studying the brittle-ductile transition and high temperature nanoindentation behaviour of tantalum.

This chapter highlights some of the nanoindentation trials performed using the MD simulation using the vision-augmented MD simulation (VAMDS) method. In this particular chapter, a particular case study was undertaken on nanoindentation trial of tantalum (Ta) on the (010), (110) and (111) orientation using a rigid tantalum indenter and a purely repulsive indenter described by a force matching embedded atom method (EAM) potential.

6.2 Brief review of literature on contact loading of tantalum

Tantalum, a BCC metal and a part of refractory metal group is a candidate material for applications in high-temperature hardware and in the electronics industry partly also because of its very high melting point (3290K) which is exceeded only by rhenium (3453K) and tungsten (3683K) thereby allowing to study the BCC peculiarities of Ta at room temperature (BCC metals typically show a BCC-type and FCC-type behaviours at about 0.15 $T_{melting}$ = 493.5 K for tantalum) [96]. Hence, there is a surge in interest in advancing the current understanding on the deformation mechanics of tantalum. However, despite the fact that nano/micro mechanical properties are scale dependent, the current pool of knowledge on the deformation behaviour of Ta is still

sparse. Consequently, there is a need to carry out an MD simulation study in this work for monitoring the atomic scale deformation processes in Ta. Exploration of this sort will help enhance our overall understanding of this notorious material which deviates in its deformation behaviour from other BCC materials.

In nature tantalum exists in either the BCC alpha phase (α-Ta) or the metastable-tetragonal beta phase (β-Ta). The α-Ta is the phase commonly found in bulk tantalum, which is ductile and exhibits higher ductility but lower electrical resistivity and hardness than β-Ta, which is brittle [97]. In a magnetron sputtering study of Ta films Myers *et al.* [98] reported that the β to α transition occurs between the temperature 638 K and 648 K. Knepper *et al.* [99] also had similar observations and indicated that β-Ta is no longer favourable when temperatures reaches in the range of 613 K to 623 K. Bulk Ta (α-Ta) resides in a BCC crystal structure and hence analysing its crystallography is rather straightforward. The closed packed planes and closed-packed directions in a BCC crystal have important implications on the deformation behaviour of the material. It is significant that in most cases that if the atomic density per unit area is highest on any crystal orientation and the distance between the two adjacent planes is farthest, then this becomes the weaker plane and is more amenable to deformation [100].

In the past, a myriad of experimental studies have been done to study the deformation behaviour of α-Ta however they haven't fully revealed the atomic mechanics of Ta. For example, Biener *et al.* [96] performed nanoindentation tests on the (010), (110) and (111) orientation of single crystal Ta to characterise the dislocation nucleation phenomenon, and their results indicated that single pop-in behaviour can be observed for the (001) orientation, but multiple pop-ins were observed on the (110) and (111) orientations. Attributing this as a general trend to all the BCC materials, they speculated that the (010) orientation of Ta as a typical example of surface which shows dislocation multiplication process, i.e. once plasticity starts, the material flows continuously and no

further pop-ins are observed. Guerrero *et al.* [101] carried out MD simulation of uniaxial compression of nanocrystalline tantalum using their *in-house* developed EAM potential function to study the elastic-plastic transition on three crystallographic directions namely, (100), (110) and (111). They concluded that the nucleation of defects along (110) of Ta was due to crystal twinning arising out of dynamical instabilities (soft phonons). They also find out that the critical stress causing the elastic-plastic transition on the (110) crystallographic direction exceeds the theoretical critical value of shear stress in Ta. α-Ta films with grain size of 10 to 30 nm prepared by magnetron sputtering on oxidised silicon substrate were recently investigated using nanoindentation [102] with a Berkovich indenter. It was found out that the plastic deformation of nanocrystalline Ta during nanoindentation is due to the crystal twinning (the location of twins being near to the edges and corners of the indent) with the threshold density limit of twins being 4×10^7 per metre resulting in a total strain of about 3.7% [102]. This finding was in contrast to a common lore whereby shear banding is considered to be the prevalent mechanism during the deformation of BCC metals.

It may thus be seen that a great amount of disparate literature exists reporting several important results on the deformation aspects of tantalum, some differing with each other. Most importantly, despite all these studies, there has been no effort made to clarify how nanoindentation of Ta is going to be influenced by its crystal orientation which mandated the need for this work.

6.3 VAMDS methodology for nanoindentation of tantalum

The MD simulation model after equilibration is shown in figure 6-1. The atoms in the Newton region directly affected by the chemical interactions were allowed to follow Newtonian dynamics (LAMMPS NVE dynamics), while atoms in a thin boundary layer were subjected to a thermostat (LAMMPS NVT dynamics) to dissipate the heat generated in the artificial volume which would have otherwise taken away by the air

during nanoindentation or lubricant (in cutting). The atoms in the indenter were kept fixed (the indenter was assumed to be an infinitely rigid body). In the literature, no potential energy function was found to allow interaction between carbon and tantalum and hence, the spherical indenter was filled with the tantalum atoms to describe the chemical interactions. An additional dummy trial was performed using the conventional manual method to ensure that this assumption is not out of order and the results obtained from this trial are also compared with the other results presented here. In this addition trial (without VAMDS), the selection of the indenter was driven from the notion that the experimental conditions often involve the presence of oxide layers which creates a passivation layer over the indenting surface.

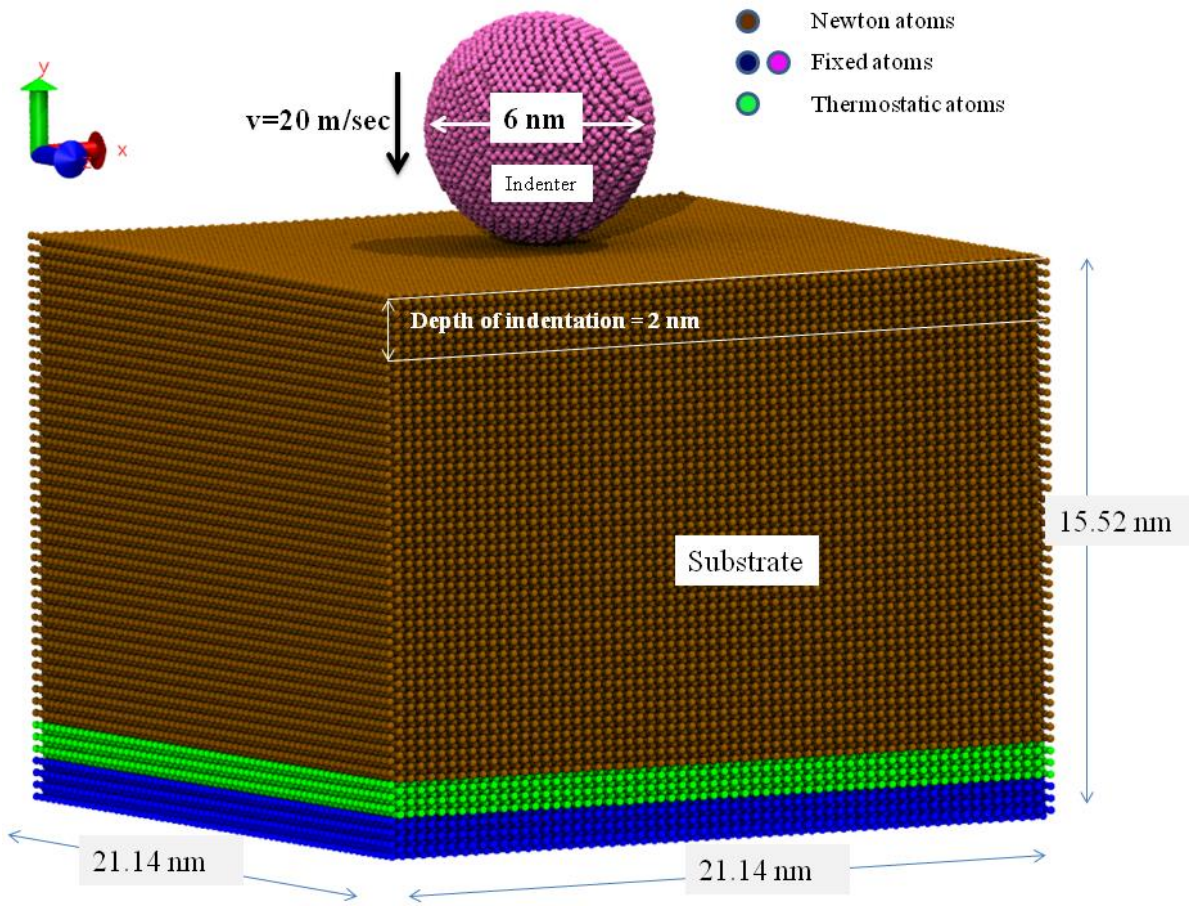

Figure 6-1: Schematic diagram of MD simulation model of the nanoindentation of tantalum.

Kelchner *et al.* [103] have used a purely spherical repulsive rigid indenter with a force potential. In this potential, each atom in the indented material interacts with the idealized indenter to experience a force of magnitude $F(r) = K(r-R)^2$ where *K* is the force constant (2 KeV/Å^3= 3204 nN/Å^2), *R* = 3 nm which is radius of the spherical indenter and *r* is the distance of atom of another species from the centre of the spherical indenter. This implies that F(r) remains repulsive as long as R > r or becomes zero otherwise. To check the sensitivity of the value of K on the *P-h* plot, an additional dummy trial by changing the value of *K* from 2 KeV/Å^3 to 1 KeV/Å^3 was also carried but the results reported here remained unchanged.

This study made use of an EAM potential proposed by Li *et al.* [104] that was developed by fitting the experimental and density-functional theory (DFT). While the details of these potential functions are readily available from their respective sources, the details of the parameters used to develop the MD simulation model in this work are shown in Table 6-1.

Table 6-1: Details used for development of the MD simulation model

Equilibrium parameter of tantalum	BCC material with a lattice constant of 3.3026Å	
Dimension of the tantalum workpiece	Crystal orientation	Number of atoms in the workpiece
21.136 nm × 15.52 nm × 21.136 nm	(010)	385,024
21.033 nm × 15.41 nm × 21.165 nm	(110)	380,952
21.033 nm × 15.44 nm × 21.018 nm	(111)	379,080
Indenter specifications	6 nm diameter rigid spherical indenter (filled with Ta atoms) having (010) crystal orientation	
Description of indenter, workpiece and cross interactions (Potential energy function used)	EAM potential developed by force matching method [104]	
Indenter and specimen surface distance (initial)	0.5 nm	
Depth of indentation	2 nm	
Speed of indentation and retraction	20 m/s = 0.02 nm/ps	
Total simulation time (Indentation+retraction)	(2+0.5 nm)/0.02 nm/ps = 125 ps×2 = 250 ps	
Timestep for each calculation	2 fs = 0.002 ps	
Total run timesteps	250/0.002 = 1,25,000	
Boundary conditions	Periodic in X and Z direction	
Ensemble used in the simulation	NVE at 10 K	

6.3.1 Calibration of the VAMDS system for nanoindentation of tantalum

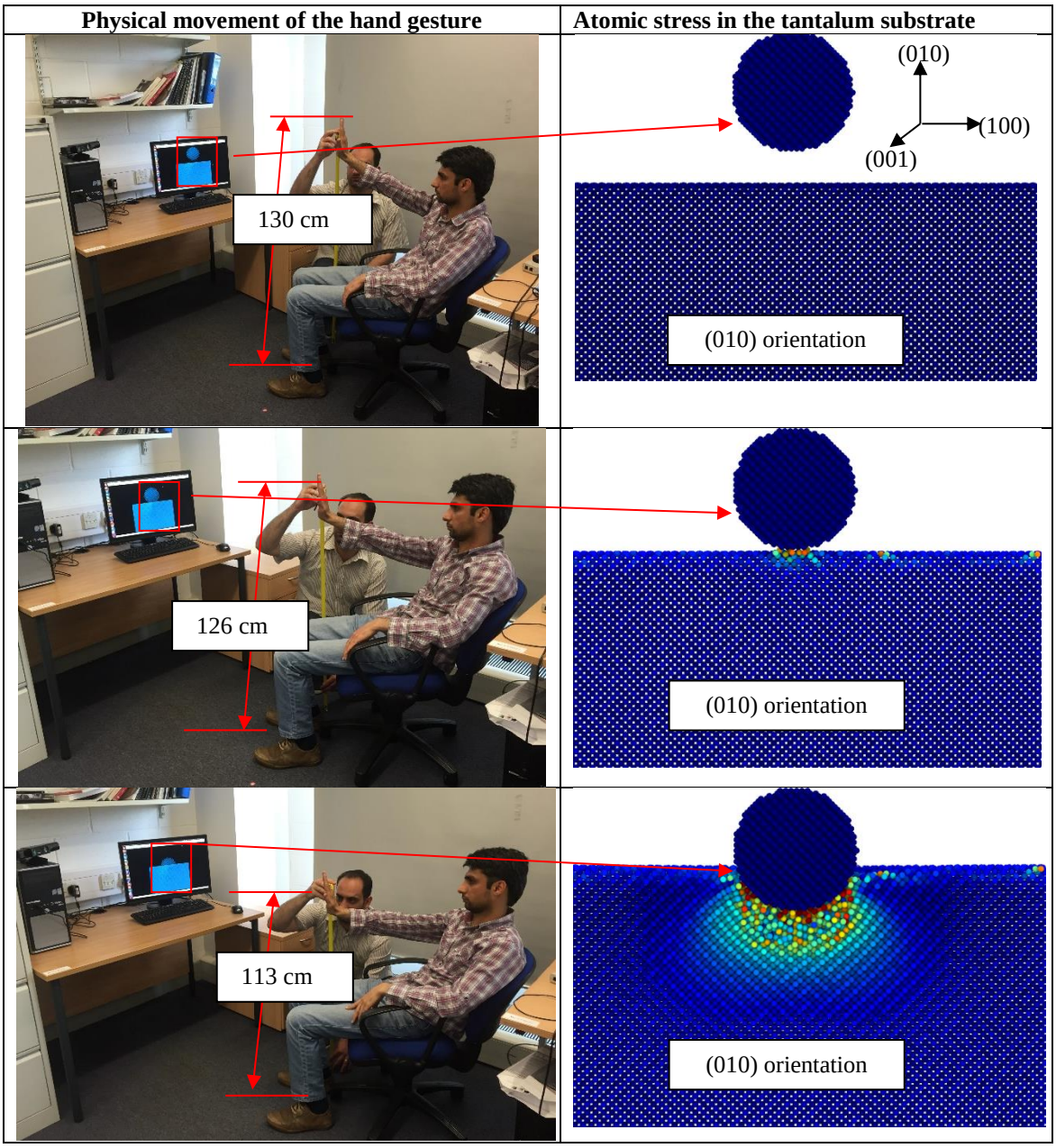

Figure 6-2: Comparison of physical movement with the movement in the MD simulation model (a) at the beginning of the simulation, (b) when the indenter establishes contact with the substrate and (c) final indentation depth was achieved.

Figure 6-2 shows the progressive physical movement of the human hand sensed by the gesture application (left column) and transformation of this physical hand movement into the corresponding displacement of the indenter into the Ta substrate (right hand column). The physical distances of the hand movements were captured through a measurement tape and were compared with the movement of the indenter in the MD

simulation model so calibrate the system (transferability of the hand movement into the equivalent displacement of the indenter). The relation between these two movements was plotted and is shown in figure 6-3. Similar to the indentation of silicon, knowing this relation was a preliminary step for calibrating the newly proposed VAMDS system.

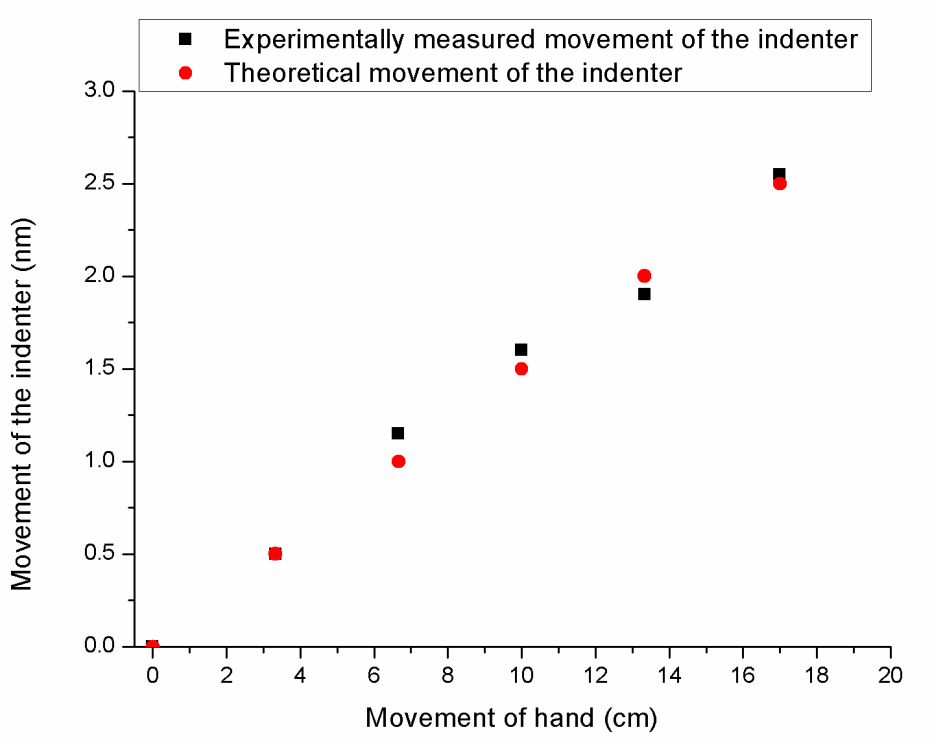

Figure 6-3: Relationship between physical movement of hand gesture and indenter in the MD model

6.4 VAMDS results for nanoindentation of tantalum

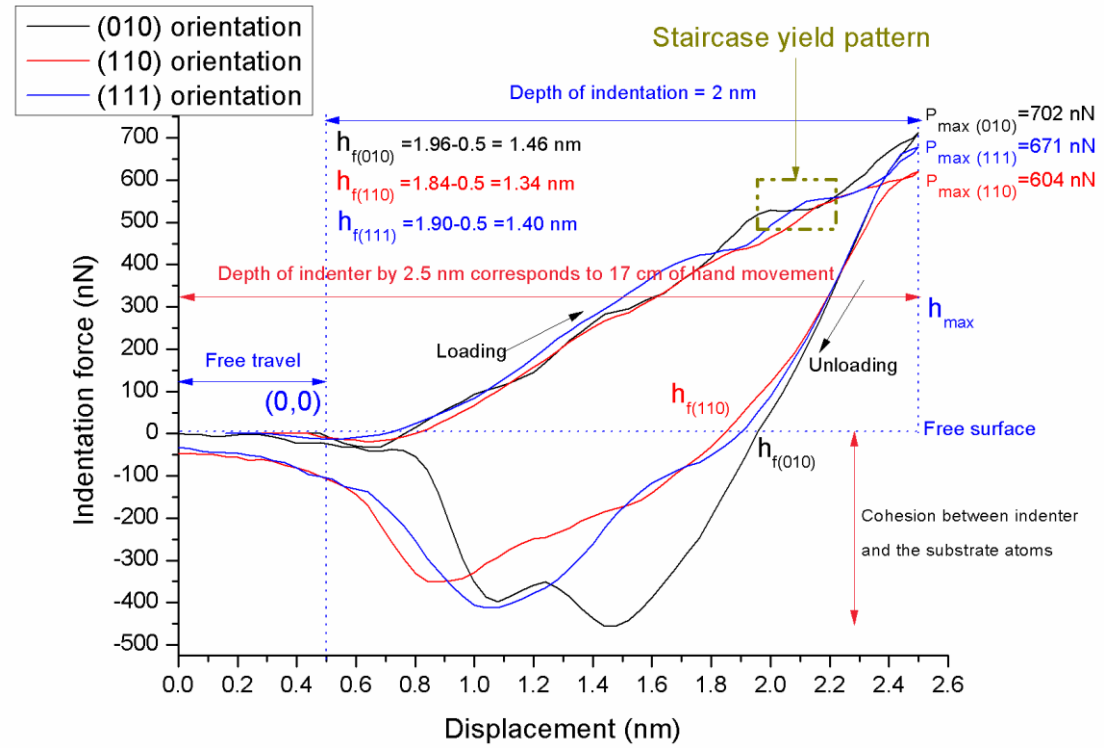

Figure 6-4: P-h plots obtained from the MD simulation for the three cases using rigid tantalum indenter

A close examination of the *P-h* plots in figure 6-4 and figure 6-5 reveals clear differences in the force necessary to deform the three crystallographic orientation of tantalum to an indentation depth of 2 nm as well as the differences in the two kind of indenters used for the simulation. The *P-h* plot for tantalum reveals that the indentation force (or energy) required to achieve a certain penetration depth in Ta is minimum on the (110) orientation and maximum on the (010) orientation while intermediate for the (111) orientation because the maximum load (~702 nN) needed to indent the (010) orientation was much higher than what was needed to indent the (110) orientation (604 nN). Also, it is quite surprising to see the cohesion component of forces during retraction stage. It appears that the (010) orientation has highest cohesion. However, it may be noted that the anisotropy for cohesion arises from the fact that a rigid tantalum indenter (010 orientations) was used for indentation meaning thereby that the same plane will have more cohesion.

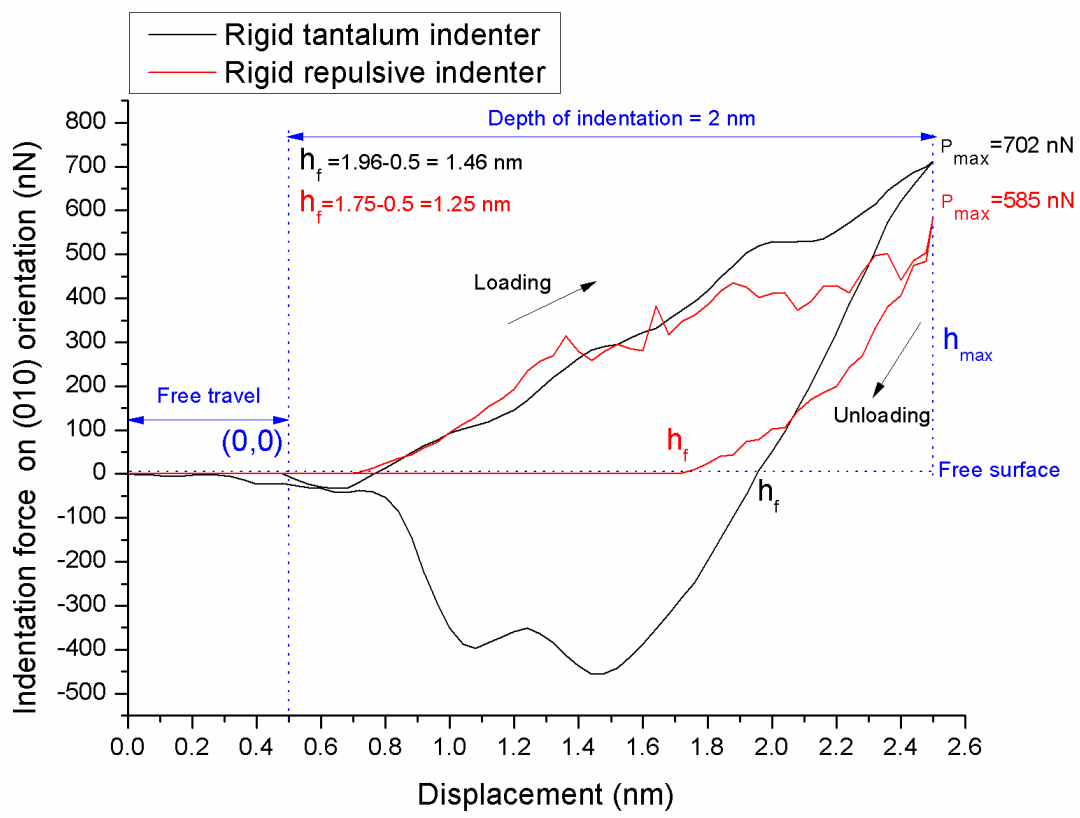

Figure 6-5: Manually performed comparison between VAMDS with a purely repulsive indenter on the (010) orientation of tantalum by keeping all the indentation parameters same but using two different kind of indenters (i) using a rigid tantalum indenter by VAMDS and (ii) a purely repulsive indenter simulated without VAMDS

Thus, the cohesion anisotropic observations visible in these plots are something which can better be confirmed using a diamond indenter. Another thing to notice is that Bahr *et al.* [105] observed that when the shear stress prior to yield is just slightly higher than the flow stress, a phenomenon referred to as "staircase yielding" prevails and one such pattern is evident on the (010) orientation which is marked appropriately in figure 6-4. The slope or stiffness (*S*) of the unloading curve obtained from the MD simulation were 1611.6 N/m for (010) orientation, 1375.2 N/m for (110) orientation and 1617.6 N/m for the (111) orientation respectively signifying the stiffness of the system for the three simulated crystal surfaces. The value of Young's modulus with the change in the crystal orientation and with the change in the indentation depth are plotted using this information in figure 6-6a and the corresponding hardness values are plotted in figure 6-6b.

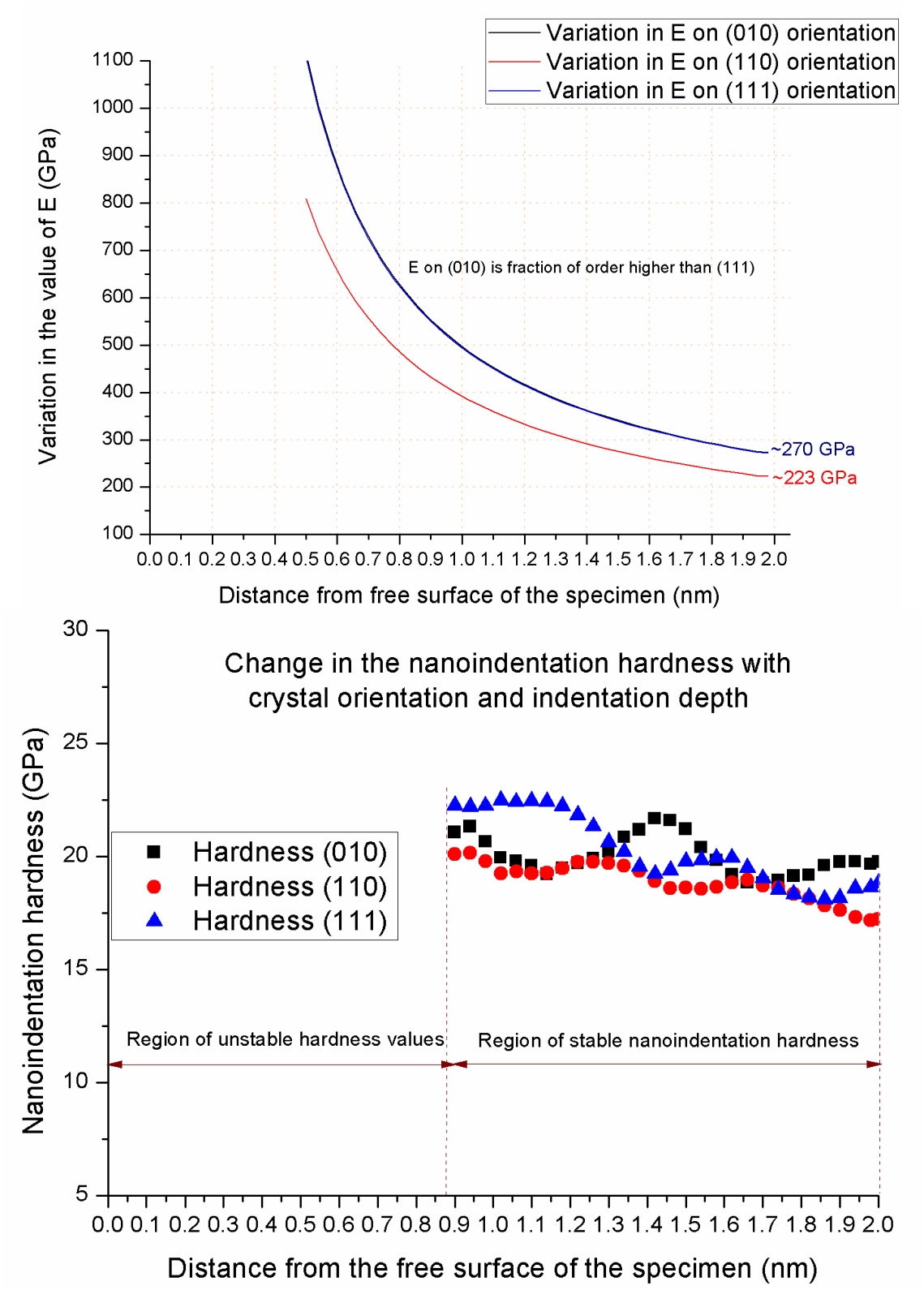

Figure 6-6: Variation in the (a) elastic modulus and (b) nanoindentation hardness of tantalum with respect to the indentation depth

Both hardness [106, 107] as well as Young's modulus [108] varies with size scale and the difference in the value of Young's modulus of tantalum on the (010) and (111)

plane at 2 nm of depth of indentation was found minimal. The combined observation from figure 6-6 suggests that the indentation size effect driven hardness as well as the elastic modulus is quite high in tantalum compared to the bulk value of the same and that obtained from elastic constants of tantalum would suggest that the order of decreasing Young's modulus should be $E_{111} > E_{110} > E_{010}$. The hardness values or the Hertzian stress underneath the indenter started stabilizing in all the three cases only after the indenter has moved by about 0.9 nm into the substrate making the hardness data calculated before this point meaningless [109]. Thus, around 0.9 nm of indentation depth is minimum needed indentation depth to get even the indentation size effect driven value of hardness.

The stabilized values of the Young's modulus suggest that the value of E on the (010) orientation is 0.02% higher than on the (111) orientation while the value of the (110) orientation is least. Analysing the hardness curve it appears that the (110) orientation shows the lowest hardness of the three orientations. Both observations are in accordance with the *P-h* plots wherein the (110) orientation showed the least steep unloading and well as loading slopes. These are quantified in table 6-2 and the hardness value obtained by purely repulsive indenter has also been compared against the value predicted by the rigid tantalum indenter for reference. The peak indentation load and residual depth of recovery were all found to align with the observations of Young's modulus i.e. least on the (110) plane and maximum on the (010) plane while intermittent on the (111) plane. Next we also noted the peak temperature in the deformation zone. The repulsive indenter seems to overestimate the temperature by a large margin from what was obtained from the rigid tantalum indenter. Moreover, the temperature in the deformation zone was found least while indenting on the (110) orientation.

Table 6-2: Summary of results obtained from the MD simulation (P-h plots)

Crystal orientation	**Remarks**	**Peak Load (nN)**	**h_f (Residual depth of recovery) (nm)**	**Average hardness (GPa) as per Oliver and Pharr method [84]**	**Peak temperature in the deformation zone (K)**
(010)	Repulsive indenter	585	1.25	18.29	251
(010)	VAMDS	702	1.46	21.4	143
(110)		671	1.34	20.5	110
(111)		604	1.4	22.3	157

6.5 Summary

This chapter presents the simulation results of nanoindentation of tantalum as a representative body centred cubic (BCC) model material system using the proposed VAMDS. With what had been somewhat a cumbersome process to do via a traditional scripting process, VAMDS facilitate the shuffling of crystal orientation and to achieve any given indentation depth merely by the hand movements swiftly. The results obtained from the testbed study can be summarized as follows:

1. Obtaining the anisotropy in the hardness and elastic modulus using classical way of doing molecular dynamics simulation would have been a relatively tedious task but with the implementation of the VAMDS, this is easily achievable, simply by using the hand gestures to create a modified atomic coordinated file and then to perform the dynamics on this file. The use of haptic device as shown in this work reduces the pain of obtaining mechanical property *via* P-h profile as

the simulation run can be restarted from any point merely by the use of hand gestures which is thus the merit of this work.

2. Using a force matching embedded atomic method (EAM) potential energy function driven molecular dynamics simulation in conjunction with 3D stress analysis in the deformation zone and application of the Oliver and Pharr method, some novel and intriguing simulated nanoindentation results are obtained concerning crystal anisotropy of tantalum. It can be seen for example that the elastic modulus obtained from elastic constants would suggest $E_{111} > E_{110} > E_{010}$. However, indentation simulation at depths of 2 nm and comparison with experiments shows that $E_{010} > E_{111} > E_{110}$. Similarly, a starkling difference was obtained in the nanoindentation hardness compared with bulk values suggesting strong indentation size effects.

Chapter 7- Conclusions and future work

This chapter is divided into three sections covering, respectively, an overall assessment of the contributions made in the thesis, the main conclusions of the work and, finally, the recommendations for future related work.

7.1 Conclusions of the research

The overall aim of the research was to develop a scheme that will facilitate users to perform the molecular simulations more institutively. Accordingly, this work focuses on studying the crystal anisotropy of silicon and tantalum observed during the nanoindentation process using the proposed VAMDS system. These two candidate materials were judiciously chosen based on the differences in the mechanism of plasticity shown by these two materials e.g. the former undergoes amorphisation (material phase change) while the later prominently shows dislocation nucleation.

Using an integrated approach of parallel molecular dynamics simulations in conjunction with visual augmentation with a many-body potential energy function, this dissertation provides a quantitative understanding of the nanoindentation process of silicon and tantalum. The distinct vision-augmented molecular dynamics simulation (VAMDS) algorithm developed in this work provides comprehensive results for thermal effects, high pressure phase transformation, influence of crystal anisotropy, indentation forces and stresses (hydrostatic and von Mises), effects not dealt with hitherto. Thus, the work was primarily aimed at developing a VAMDS which was tested by performing a case study on nanoindentation of silicon and tantalum. It was remarkably challenging yet innovative because it will open up new horizons for the development of new knowledge by building a clear base to enable design and creation of novel materials. This was achieved through a systematic design approach integrating the use of a haptic device that fed the data of hand gestures to the simulator. Aside explaining various aspects of

the hardware, design and development of this vision-augmented technique, following points can be concluded based on the aforementioned discussions:

1. Obtaining the variation in the hardness and elastic modulus using classical way of doing molecular dynamics simulation would have been a relatively tedious task but with the implementation of the VAMDS, this is easily achievable. The use of haptic device as shown in this work reduces the pain of obtaining mechanical property *via* P-h profile as the simulation run can be restarted from any point merely by the use of hand gestures which is the major novelty of this work.
2. The mechanism of ductility in silicon during its nanoindentation and the observed plasticity occurs due to the high pressure phase transformation (HPPT) that is driven by stress rather than temperature. For HPPT to occur in silicon, the von Mises and Tresca stress for the (110) orientation were found maximum while the (010) orientation showed least values whereas the (111) orientation showed somewhat an intermittent value.
3. At an indentation depth of 2 nm, it was seen that the unloading curve for the (110) and the (111) substrate follows power law whereas the unloading curve on the (010) substrate showed an elbow which was found related with the formation of a-Si upon the retraction of the indenter on the (010) orientation only. Furthermore, the elastic constants of silicon varied in the order of $E_{111} > E_{110} > E_{010}$.
4. Using a force matching embedded atomic method (EAM) potential energy function driven molecular dynamics simulation in conjunction with 3D stress analysis in the deformation zone and application of the Oliver and Pharr method, some novel and intriguing simulated nanoindentation results are obtained concerning crystal anisotropy of tantalum. It can be seen for example that the

elastic modulus obtained from elastic constants would suggest $E_{111} > E_{110} > E_{010}$. However, indentation simulation at depths of 2 nm and comparison with experiments shows that $E_{010} > E_{111} > E_{110}$. Similarly, a starkling difference was obtained in the nanoindentation hardness compared with bulk values suggesting strong indentation size effects.

7.2 Research contributions

In this work, two case studies were performed on silicon and tantalum using state-of-the-art potential energy functions with the help of VAMDS. Until now, the study of crucial properties like anisotropy at the atomic scale requires writing time consuming scripts. In an attempt to avoid the laborious efforts associated with writing the scripts, this work shows one of the tested pathways to overcome this limitation. . Directing a simulation via an interacting mechanism using merely the hand gestures using the fundamental principles of computer vision to bring the two-bodies together to perform the molecular dynamics is a major novelty and contribution of this research. This aligns well with the objectives of this research i.e. VAMDS helped the user to institutively become the part of the simulation thereby uncovering the black-box of the MD simulation. Hence, VAMDS was developed as a virtual environment tool that can offer exploration of complex energy landscapes by allowing the user to directly interact with the simulated molecular system. The system is novel in its concept as it enables the user to directly manipulate the atomic structures on the screen, in three-dimensional (3D) space using hand gestures, allowing the exploration and visualisation of molecular interactions at different relative conformations. The hand gestures are used to pick and place atoms on the screen allowing thereby the ease of carrying out molecular dynamics simulation in a more convenient way. The end result is that users with limited expertise in developing molecular structures can now do so easily and intuitively by the use of body gestures to interact with the simulator to study the system in question. The

proposed system was tested by simulating the crystal anisotropy of crystalline silicon and tantalum during nanoindentation. With this aim, this thesis has provided further insights into the current state of knowledge in the field of nanoindentation of silicon and tantalum by making use of the most recent potential energy functions. The novelty and contribution arising from this research lies in:

- Development of the hardware and a design approach to use the haptic device for carrying out the molecular dynamics simulation.
- Using the proposed VAMDS approach for studying the crystal anisotropy of silicon and tantalum by developing a state-of-the-art molecular dynamics model involving state-of-the-art potential energy functions like screening bond order potential and embedded atomic method (EAM) potential.
- It is the first work using the newly proposed screened bond order potential function to demystify the mechanisms of plasticity of silicon occurring during the process of nanoindentation.
- All the simulation results were duly validated by making use of the Oliver-Pharr method to quantify the elastic modulus and hardness of the materials studied via VAMDS.

7.3 Recommendations for future work

The indentation contact behaviour of materials is characterised by combination of elastic, elastic-plastic deformation and fracture. However, there are two main approaches to the mechanics of indentation depending upon the whether the accommodation is by deformation or by fracture. Considering the MD simulation, if the contact force is applied to a material then constituent atoms will undergo reconfiguration from its original state, deforming the initial contact or near contact bonds in the process. If the bonds return to the original configuration as the applied load

is unloaded, then the deformation is elastic. If however, the bonds stay deformed upon unloading then the deformation could be described as elastic-plastic or plastic. Thus, plastic deformation can be characterised by permanent displacements of atoms. However, if those few broken bonds are not reorganized then fracture can occur. The bulk material response under indentation is a function of the individual deformations of the bonds and can therefore be combination of elastic, elastic-plastic deformation and fracture. Since MD simulation is an important theoretical technique to understand the surface and sub-surface changes in materials, the current study has been motivated partly by the identification of initial stages of yielding and fracture mechanism, phase transformation, dislocation monitoring and differentiate the types of dislocation nucleation and its motion.

An improved understanding of the physical mechanisms underpinning the response of silicon and tantalum during material property will enable us in a better position to deploy these materials in a range of applicants involving, refractory conditions, nuclear and space applications. Evaluation of properties such as hardness and elastic modulus and the implication of crystal anisotropy on these properties is of paramount importance to efficiently place these materials in an engineering application. Although we have made advances in our understanding on some of the physical mechanisms, this is still a grey area of current and future research. Since the term miniaturisation has been coined, many classical phenomena have undergone series of refinements owing primarily to the fact that the behaviour of material changes with the reduction in scale [110]. Apparently, the current canon of experimental facilities are not either easily available in public domain or are not sufficiently well advanced to capture all the mechanisms (dislocation nucleation, motion, etc.), competing within the atomic scale regime. Consequently, the assemblage of knowledge from several distinct disciplines including chemistry, physics, material science, and computing science has resulted in the

development of ever improving simulation techniques which are capable to capture these phenomena's to provide phenomenal insights of dislocation physics. The relationships among crystal orientation, dislocation nucleation and reactions and the resulting plasticity at nanoscale is a difficult bit to be understood by the state-of-the-art experimental studies alone. Detailed information on the atomic level changes leading to changes observed at macroscale can appropriately be obtained by MD simulation. In this work, a relatively simple yet an appropriate modelling approach has provided multiple pathways to understand the origins of anisotropy. The potential to tap this effect can result in significant engineering applications and is an area which needs practical and experimental realization. Consequently, the purpose for which MD simulation was carried out has provided the direction to use this knowledge in the experimental work; therefore there is an opportunity for developing richer theoretical models and at the same time the quantitative verification of the dislocation density is possible with the usage of transmission electron microscopy. This work has opened up opportunities for a number of commercial, technological and scientific developments, some of which are outlines in the following sections:

7.3.1 Development of a force field or a potential function

In future work, the use of VAMDS first of all will be readily useful for the development of a force-field. It is now possible to bring two atoms close or take them away from each other and observe the cohesive energy for the system. This can facilitate tuning of the potential parameters in a very easy way to perform the test calculations which could be used to develop a force-field eventually.

7.3.2 Manual creation of defects and study of wear

In future work, the use of MD can be extended to study contact loading in such a way that the microstructure of the material can be varied through the introduction of lattice defects to compare the performance of defect structures. This can more conveniently be accomplished by the use of proposed VAMDS method.

7.3.3 Development of enhanced MD software

Currently available MD packages are not dedicated to elucidating nanoindentation. At the moment, not only a great deal of computational power is needed but also the potential functions available to describe the materials being simulated are quite limited. This is probably the main reason why commercialization of MD tools for manufacturing and material characterisation has not been possible thus far. There is a strong need to develop a generalized formalism of potential function so that it can describe other useful materials such as glass, quartz, tungsten carbide and boron carbide, and commercial software able to simulate these engineering materials could be designed and developed using the information provided in this thesis.

7.3.4 Effects of coolant and coatings

Due to the limitations of time and the lack of potential functions, the effect of environment during nanoindentation was not studied in the current work. The presence of a coolant will certainly influence the tribo-chemistry of the indenter and studying its effect will help develop further understanding on this front.

7.3.5 Optimization of indentation probe

It was realized from this study that anisotropy can play an important role in influencing the process mechanics of nanoindentation. Not only does this influence the behaviour of

plastic deformation of the substrate but they should also influence the life of the indentation probe (diamond). A theoretical analysis to optimize this would be too complex, but MD simulation analysis would be a convenient method of optimizing tool geometry to develop the most efficient probe geometry.

7.3.6 Sensitivity and least count of the haptic device

As this was a preliminary study, the sensitivity of the equipment under different climatic, geographic and temperature conditions were not tested. It could be a worthier future work to test the sensitivity of the VAMDS system under various environmental conditions. Furthermore, the precision of the movement reflecting the least count of the movement of the indenter in the MD system would help to enhance the positioning accuracy and data characterisation obtained from the system as a part of future work.

References

1. http://www.kryshiggins.com/thoughts-on-designing-kinect-based-experiences/. accessed on 2nd September 2014.
2. PrimeSense, *NITE CONTROLS USER GUIDE*. 2011, Primesense Inc. p. 10.
3. Bar-Cohen, Y., *Topic 1 Introduction.* 2004.
4. Mistry, P., P. Maes, and L. Chang. *WUW-wear Ur world: a wearable gestural interface*. in *CHI'09 extended abstracts on Human factors in computing systems*. 2009. ACM.
5. Fermeglia, M. and S. Pricl, *Multiscale molecular modeling in nanostructured material design and process system engineering.* Computers & Chemical Engineering, 2009. **33**(10): p. 1701-1710.
6. Svaneborg, C., *LAMMPS framework for dynamic bonding and an application modeling DNA.* Computer Physics Communications, 2012. **183**(8): p. 1793-1802.
7. Aragones, J., et al., *Free energy calculations for molecular solids using GROMACS.* The Journal of Chemical Physics, 2013. **139**(3): p. 034104.
8. Aragones, J., C. Valeriani, and C. Vega, *Note: Free energy calculations for atomic solids through the Einstein crystal/molecule methodology using GROMACS and LAMMPS.* The Journal of Chemical Physics, 2012. **137**(14): p. 146101.
9. Mistry, P. and P. Maes. *SixthSense: a wearable gestural interface*. in *ACM SIGGRAPH ASIA 2009 Sketches*. 2009. ACM.
10. Mistry, P. and P. Maes, *Augmenting sticky notes as an i/o interface*, in *Universal Access in Human-Computer Interaction. Intelligent and Ubiquitous Interaction Environments*. 2009, Springer. p. 547-556.
11. Mistry, P., et al. *Blinkbot: look at, blink and move*. in *Adjunct proceedings of the 23nd annual ACM symposium on User interface software and technology*. 2010. ACM.
12. Mistry, P. and P. Maes. *Mouseless*. in *Adjunct proceedings of the 23nd annual ACM symposium on User interface software and technology*. 2010. ACM.
13. Taylor, T. and D.E. Johnson. *Tangible simulations Generalized haptic devices for human-guided computer simulations*. in *Collaboration Technologies and Systems (CTS), 2013 International Conference on*. 2013. IEEE.
14. Ricci, A., et al., *Haptic-driven applications to molecular modeling: state-of-the-art and perspectives.* Future medicinal chemistry, 2012. **4**(10): p. 1219-1228.
15. Dreher, M., et al., *Interactive molecular dynamics: scaling up to large systems.* Procedia Computer Science, 2013. **18**: p. 20-29.
16. Haag, M.P. and M. Reiher, *Studying chemical reactivity in a virtual environment.* Faraday discussions, 2014.
17. Chen, C.-T., et al., *An interactive nanomanipulation visualization based on molecular dynamics simulation and virtual reality.* Transactions of the Canadian Society for Mechanical Engineering, 2013. **37**(3): p. 991-1000.
18. Glowacki, D.R., et al., *A GPU-accelerated immersive audio-visual framework for interaction with molecular dynamics using consumer depth sensors.* Faraday discussions, 2014.
19. Waldon, S.M., et al., *SketchBio: a scientist's 3D interface for molecular modeling and animation.* BMC bioinformatics, 2014. **15**(1): p. 334.
20. Heinrich, J., M. Burch, and S.I. O'Donoghue, *On the Use of 1D, 2D, and 3D Visualisation for Molecular Graphics.*

21. Férey, N., et al. *A VR framework for interacting with molecular simulations*. in *Proceedings of the 2008 ACM symposium on Virtual reality software and technology*. 2008. ACM.
22. Bolopion, A., et al., *Comparing position and force control for interactive molecular simulators with haptic feedback.* Journal of Molecular Graphics and Modelling, 2010. **29**(2): p. 280-289.
23. Bolopion, A., et al. *Haptic feedback for molecular simulation*. in *Intelligent Robots and Systems, 2009. IROS 2009. IEEE/RSJ International Conference on*. 2009. IEEE.
24. Bolopion, A., et al. *Haptic molecular simulation based on force control*. in *Advanced Intelligent Mechatronics (AIM), 2010 IEEE/ASME International Conference on*. 2010. IEEE.
25. Sun, H., M. Li, and Y. Xu, *molvie: an interactive visualization environment for molecular structures.* Computer methods and programs in biomedicine, 2003. **71**(1): p. 85-90.
26. Hirst, J.D., D.R. Glowacki, and M. Baaden, *Molecular simulations and visualization: introduction and overview.* Faraday discussions, 2014. **169**: p. 9-22.
27. Sharma, K., I. Moon, and S.G. Kim, *Depth estimation of features in video frames with improved feature matching technique using Kinect sensor.* Optical Engineering, 2012. **51**(10): p. 107002-1-107002-11.
28. Wang, Y., et al. *Kinect based dynamic hand gesture recognition algorithm research*. in *Intelligent Human-Machine Systems and Cybernetics (IHMSC), 2012 4th International Conference on*. 2012. IEEE.
29. Han, J., et al., *Enhanced computer vision with microsoft kinect sensor: A review.* Cybernetics, IEEE Transactions on, 2013. **43**(5): p. 1318-1334.
30. Raheja, J.L., A. Chaudhary, and K. Singal. *Tracking of fingertips and centers of palm using kinect*. in *Computational intelligence, modelling and simulation (CIMSiM), 2011 third international conference on*. 2011. IEEE.
31. Novák-Marcinčin, J., *Combination of Simulation Software and Virtual Reality for Technological Workplaces Design.*
32. Hamza-Lup, F.G. and I. Sopin. *Haptics and Extensible 3D in Web-Based Environments for E-Learning and Simulation*. in *WEBIST (1)*. 2008.
33. Salvadori, A., et al., *Moka: Designing a Simple Scene Graph Library for Cluster-Based Virtual Reality Systems*, in *Augmented and Virtual Reality*. 2014, Springer. p. 333-350.
34. Salvadori, A., et al., *Graphical Interfaces and Virtual Reality for Molecular Sciences*, in *Reference Module in Chemistry, Molecular Sciences and Chemical Engineering*. 2014, Elsevier.
35. Xu, S., et al. *Immersive visualisation of nano-indentation simulation of cu*. in *Recent Advances in Computational Science and Engineering, World Scientific, Singapore. Proceedings of the International Conference on Scientific and Engineering Computation (IC-SEC) ISBN*. 2002. World Scientific.
36. Vormoor, O., *Quick and easy interactive molecular dynamics using Java3D.* Computing in Science & Engineering, 2001. **3**(5): p. 98-104.
37. Son, W., et al. *Interactive dynamic simulation using haptic interaction*. in *Intelligent Robots and Systems, 2000.(IROS 2000). Proceedings. 2000 IEEE/RSJ International Conference on*. 2000. IEEE.
38. Delalande, O., et al., *Complex molecular assemblies at hand via interactive simulations.* Journal of computational chemistry, 2009. **30**(15): p. 2375-2387.

39. Limet, S., M. Poquet, and S. Robert, *Modulight: A Framework for Efficient Dynamic Interactive Scientific Visualization.* Procedia Computer Science, 2014. **29**: p. 692-702.
40. Sasakura, M., A. Kotaki, and J. Inada. *A 3D molecular visualization system with mobile devices*. in *Information Visualisation (IV), 2011 15th International Conference on*. 2011. IEEE.
41. Sharma, A., et al., *Immersive and interactive exploration of billion-atom systems.* Presence: Teleoperators and Virtual Environments, 2003. **12**(1): p. 85-95.
42. Meier, K., et al., *3D Visualization of Molecular Simulations in High-performance Parallel Computing Environments.* Molecular Simulation, 2004. **30**(7): p. 469-477.
43. Promyoo, R., H. El-Mounayri, and X. Yang, *MOLECULAR DYNAMICS SIMULATION OF NANOMETRIC CUTTING.* Machining Science and Technology, 2010. **14**(4): p. 423-439.
44. Alder, B.J. and T.E. Wainwright, J. Chem. Phys., 1957. **1208**(27).
45. Bhushan, B., J.N. Israelachvili, and U. Landman, *Nanotribology - Friction, Wear and Lubrication at the Atomic-Scale.* Nature, 1995. **374**(6523): p. 607-616.
46. Cai, W., J. Li, and S. Yip, *1.09 - Molecular Dynamics*, in *Comprehensive Nuclear Materials*, J.M.K. Editor-in-Chief: Rudy, Editor. 2012, Elsevier: Oxford. p. 249-265.
47. Komanduri, R. and L. Raff, *A review on the molecular dynamics simulation of machining at the atomic scale.* Proceedings of the Institution of Mechanical Engineers, Part B: Journal of Engineering Manufacture, 2001. **215**(12): p. 1639-1672.
48. Sen, D., et al., *Atomistic Study of Crack-Tip Cleavage to Dislocation Emission Transition in Silicon Single Crystals.* Physical Review Letters, 2010. **104**(23): p. 235502.
49. Plimpton, S.J. and A.P. Thompson, *Computational aspects of many-body potentials (DOI:10.1557/mrs.2012.96).* MRS Bulletin, 2012. **37**: p. 513-521.
50. Ikawa, N., et al., *An Atomistic Analysis of Nanometric Chip Removal as Affected by Tool-Work Interaction in Diamond Turning.* CIRP Annals - Manufacturing Technology, 1991. **40**(1): p. 551-554.
51. Tersoff, J., *New empirical approach for the structure and energy of covalent systems.* Physical Review B, 1988. **37**(12): p. 6991.
52. Tersoff, J., *Empirical interatomic potential for silicon with improved elastic properties.* Physical Review B, 1988. **38**(14): p. 9902.
53. Tersoff, J., *Modeling solid-state chemistry: Interatomic potentials for multicomponent systems.* Physical Review B, 1989. **39**(8): p. 5566.
54. Tersoff, J., *Erratum: Modeling solid-state chemistry: Interatomic potentials for multicomponent systems.* Physical Review B, 1990. **41**(5): p. 3248.
55. Tersoff, J., *Carbon defects and defect reactions in silicon.* Physical Review Letters, 1990. **64**(15): p. 1757.
56. Tersoff, J., *Chemical order in amorphous silicon carbide.* Physical Review B, 1994. **49**(23): p. 16349.
57. Erhart, P. and K. Albe, *Analytical potential for atomistic simulations of silicon, carbon, and silicon carbide.* Physical Review B, 2005. **71**(3): p. 035211.
58. Erhart, P. and K. Albe, *Analytical potential for atomistic simulations of silicon, carbon, and silicon carbide.* Physical Review B, 2005. **71**(3): p. -.

59. Kumagai, T., et al., *Development of bond-order potentials that can reproduce the elastic constants and melting point of silicon for classical molecular dynamics simulation.* Computational Materials Science, 2007. **39**(2): p. 457-464.
60. Pastewka, L., et al., *Describing bond-breaking processes by reactive potentials: Importance of an environment-dependent interaction range.* Physical Review B, 2008. **78**(16): p. 161402.
61. Pastewka, L., et al., *Screened empirical bond-order potentials for Si-C.* Physical Review B, 2013. **87**(20): p. 205410.
62. Pastewka, L., et al., *Bond order potentials for fracture, wear, and plasticity.* MRS Bulletin-Three decades of many-body potentials in materials research, 2012. **37**(5): p. 493-503.
63. Goel, S., et al., *Nanoindentation of polysilicon and single crystal silicon: Molecular dynamics simulation and experimental validation.* Journal of Physics D: Applied Physics, 2014. **47**(27): p. 275304.
64. Pastewka, L., et al., *Anisotropic mechanical amorphization drives wear in diamond.* Nature Materials, 2011. **10**(1): p. 34-38.
65. Luo, X., *High Precision Surfaces Generation: Modelling, Simulation and Machining Verification*, in *Mechanical Engineering*. 2003, Leeds Metropolitan University: Leeds.
66. Notman, R. and J. Anwar, *Breaching the skin barrier — Insights from molecular simulation of model membranes.* Advanced Drug Delivery Reviews, 2012(0).
67. Pizani, P.S., et al., *Ductile and brittle modes in single-point-diamond-turning of silicon probed by Raman scattering.* Journal of Materials Science Letters, 1999. **18**(14): p. 1185-1187.
68. Stukowski, A., *Structure identification methods for atomistic simulations of crystalline materials.* Modelling and Simulation in Materials Science and Engineering, 2012. **20**(4): p. 045021.
69. Cheong, W.C.D. and L.C. Zhang, *Molecular dynamics simulation of phase transformations in silicon monocrystals due to nano-indentation.* Nanotechnology, 2000. **11**(3): p. 173.
70. Komanduri, R., N. Chandrasekaran, and L.M. Raff, *Molecular dynamics simulation of the nanometric cutting of silicon.* Philosophical Magazine Part B, 2001. **81**(12): p. 1989 - 2019.
71. http://isaacs.sourceforge.net/phys/rdfs.html, *g(r) RDF Explanation accessed on 10/3/2011*.
72. in't Veld, P.J., S.J. Plimpton, and G.S. Grest, *Accurate and efficient methods for modeling colloidal mixtures in an explicit solvent using molecular dynamics.* Computer Physics Communications, 2008. **179**(5): p. 320-329.
73. Chen, J.X. and C. Chen, *Guide to graphics software tools*. 2003: Springer.
74. Willighagen, E. and M. Howard, *Fast and scriptable molecular graphics in web browsers without Java3D.* 2007.
75. Willighagen, E.L., *Processing CML conventions in Java.* Internet Journal of Chemistry, 2001. **4**(4): p. 1099-8292.
76. Herráez, A., *How to use Jmol to study and present molecular structures*. Vol. 1. 2007: Lulu. com.
77. Herraez, A., *Biomolecules in the computer: Jmol to the rescue.* Biochemistry and Molecular Biology Education, 2006. **34**(4): p. 255-261.
78. Stukowski, A., *Visualization and analysis of atomistic simulation data with OVITO–the Open Visualization Tool.* Modelling and Simulation in Materials Science and Engineering, 2010. **18**(1).

79. Stukowski, A. and K. Albe, *Extracting dislocations and non-dislocation crystal defects from atomistic simulation data.* Modelling and Simulation in Materials Science and Engineering, 2010. **18**(8): p. 085001.
80. Stukowski, A. and A. Arsenlis, *On the elastic–plastic decomposition of crystal deformation at the atomic scale.* Modelling and Simulation in Materials Science and Engineering, 2012. **20**(3): p. 035012.
81. Stukowski, A., V.V. Bulatov, and A. Arsenlis, *Automated identification and indexing of dislocations in crystal interfaces.* Modelling and Simulation in Materials Science and Engineering, 2012. **20**(8): p. 085007.
82. Goel, S., A. Agrawal, and N.H. Faisal, *Can a carbon nano-coating resist metallic phase transformation in silicon substrate during nanoimpact?* Wear, 2014. **315**(1-2): p. 38-41.
83. Goel, S., et al., *Molecular dynamics simulation of nanoindentation of Fe3C and Fe4C.* Materials Science and Engineering: A, 2014. **597**(0): p. 331-341.
84. Oliver, W.C. and G.M. Pharr, *Improved technique for determining hardness and elastic modulus using load and displacement sensing indentation experiments.* Journal of Materials Research, 1992. **7**(6): p. 1564-1583.
85. Mylvaganam, K. and L.C. Zhang, *Nanotwinning in monocrystalline silicon upon nanoscratching.* Scripta Materialia, 2011. **65**(3): p. 214-216.
86. Kim, D. and S. Oh, *Atomistic simulation of structural phase transformations in monocrystalline silicon induced by nanoindentation.* Nanotechnology, 2006. **17**(9): p. 2259.
87. Jang, J.-i., et al., *Indentation-induced phase transformations in silicon: influences of load, rate and indenter angle on the transformation behavior.* Acta Materialia, 2005. **53**(6): p. 1759-1770.
88. Shibata Y., F.S., Makino E. and Ikeda M., *Ductile-regime turning mechanism of single-crystal silicon.* Precision Engineering, 1996. **18**: p. 129-137.
89. Goel, S., *A topical review on "The current understanding on the diamond machining of silicon carbide".* Journal of Physics D: Applied Physics, 2014. **47**(24): p. 243001.
90. Goel, S., et al., *Diamond machining of silicon: A review of advances in molecular dynamics simulation.* International Journal of Machine Tools and Manufacture, 2015. **88**(0): p. 131-164.
91. Ravindra, D., *Ductile mode material removal of ceramics and semiconductors*, in *Department of Mechanical and Aeronautical Engineering*. 2011, Western Michigan University: Michigan. p. 312.
92. Gogotsi, Y.G., A. Kailer, and K.G. Nickel, *Materials: Transformation of diamond to graphite.* Nature, 1999. **401**(6754): p. 663-664.
93. Goel, S., X. Luo, and R.L. Reuben, *Wear mechanism of diamond tools against single crystal silicon in single point diamond turning process.* Tribology International, 2013. **57**(0): p. 272-281.
94. O'Connor, B.P., Marsh, E. R. and Couey, J. A., *On the effect of crystallographic orientation on ductile material removal in silicon.* Precision Engineering, 2005. **29**: p. 124-132.
95. Zhao, H., et al., *Molecular Dynamics Simulation of the Crystal Orientation and Temperature Influences in the Hardness on Monocrystalline Silicon.* Journal of Nanomaterials, 2014. **2014**: p. 8.
96. Biener, M.M., et al., *Dislocation nucleation in bcc Ta single crystals studied by nanoindentation.* Physical Review B, 2007. **76**(16): p. 165422.
97. Cao, Z., et al., *The rate sensitivity and plastic deformation of nanocrystalline tantalum films at nanoscale.* Nanoscale Research Letters, 2011. **6**(1): p. 1-6.

98. Myers, S., et al., *The β to α phase transition of tantalum coatings deposited by modulated pulsed power magnetron sputtering.* Surface and Coatings Technology, 2013. **214**(0): p. 38-45.
99. Knepper, R. and S.P. Baker, *Coefficient of thermal expansion and biaxial elastic modulus of β phase tantalum thin films.* Applied Physics Letters, 2007. **90**(18): p. 181908-181908-3.
100. Goel, S., et al., *Anisotropy of single-crystal 3C–SiC during nanometric cutting.* Modelling and Simulation in Materials Science and Engineering, 2013. **21**(6): p. 065004.
101. Guerrero, O. and M. Marucho, *Elastic-Plastic Transition under Uniaxial Stress BCC Tantalum.* Journal of Materials Science and Engineering B, 2013. **3**(3): p. 153-160.
102. Wang, Y., et al., *Deformation twinning during nanoindentation of nanocrystalline Ta.* Applied Physics Letters, 2005. **86**(10): p. 101915.
103. Kelchner, C.L., S.J. Plimpton, and J.C. Hamilton, *Dislocation nucleation and defect structure during surface indentation.* Physical Review B, 1998. **58**(17): p. 11085.
104. Li, Y., et al., *Embedded-atom-method tantalum potential developed by the force-matching method.* Physical Review B, 2003. **67**(12): p. 125101.
105. Bahr, D.F., D.E. Kramer, and W.W. Gerberich, *Non-linear deformation mechanisms during nanoindentation.* Acta Materialia, 1998. **46**(10): p. 3605-3617.
106. Cao, Y., et al., *Nanoindentation measurements of the mechanical properties of polycrystalline Au and Ag thin films on silicon substrates: Effects of grain size and film thickness.* Materials Science and Engineering: A, 2006. **427**(1–2): p. 232-240.
107. Cao, Z., et al., *Indentation size effects on the creep behavior of nanocrystalline tetragonal Ta films.* Scripta Materialia, 2009. **60**(6): p. 415-418.
108. Ao, Z.M., S. Li, and Q. Jiang, *The determination of Young's modulus in noble metal nanowires.* Applied Physics Letters, 2008. **93**(8): p. -.
109. Chen, S. and F. Ke, *MD simulation of the effect of contact area and tip radius on nanoindentation.* Science in China Series G: Physics, Mechanics and Astronomy, 2004. **47**(1): p. 101-112.
110. Geim, A.K. and K.S. Novoselov, *The rise of graphene.* Nature Materials, 2007. **6**(3): p. 183-191.